Dalton Transactions



PERSPECTIVE

View Article Online
View Journal | View Issue



Cite this: *Dalton Trans.*, 2025, **54**, 10504

Received 24th April 2025, Accepted 28th May 2025 DOI: 10.1039/d4dt03357d

rsc.li/dalton

Reactive main group metal complexes of the neutral NNNN macrocycle, Me₄TACD

Priyabrata Ghana, Da Louis J. Morris Db and Jun Okuda D*c

Currently, there is considerable interest in introducing molecularly defined main group metal compounds as precursors and model complexes of homogeneous catalysts for various bond cleavage and forming transformations. With a focus on the *NNNN* macrocyclic ligand Me₄TACD (*N,N',N'',N'''*-tetramethyl-1,4,7,10-tetraazacyclododecane), this review summarizes the versatility of the ligand Me₄TACD for the stabilization of reactive main group s- and p-block (group 1, 2, 12–14) metals. Metal hydrides, hydrocarbyls and silyls are often monomeric and catalyze alkene hydrofunctionalisations. In contrast to the rich coordination chemistry of d- and f-block transition metals using a plethora of ligands, main group metals still leave room for new structures and reactivities, aligning with the current efforts to develop a systematic understanding in s- and p-block metal-ligand combinations.

1. Introduction

Commonly, reactive main group metal fragments are stabilized by anionic ligands of the general type $[L_lX_x]$ (L = two-electron ligand, l = 0-4; X = one-electron ligand, x = 1-4), which exhibit sterically bulky substituents. N-Heterocyclic carbene derivatives are often employed in this regard as neutral L-type ligands. Neutral multidentate N- and O-donor ligands of the general type L_n can provide access to soluble and reactive molecular s-block complexes. Macrocyclic N-donor ligands have seen less widespread use in the main group chemistry.

The macrocyclic tetraamine ligand, Me₄TACD (*N,N',N'',N'',N'''*-tetramethyl-1,4,7,10-tetraazacyclododecane, also called 12-TMC or Me₄cyclen) has been used in the coordination chemistry of 3d metals as a redox innocent supporting ligand. It was first developed in 1982 to study the effect of *N*-methylation of cyclic polyamines on the coordination number of late transition metals such as Ni and Cu and extensively to study reactive (di)oxygen species during O₂ activation at Cr, Mn, Fe, Co, Ni, and Cu centers. ^{21,22} This review summarizes the use of Me₄TACD as a versatile supporting ligand for the study of main group metal centers featuring reactive ligands such as hydride and organyls, mostly as cations. Such species are often of low-nuclearity, often monomeric and allow to study the inherent property of main group metal-ligand interaction. Since some group 1 and 2 metals are abundant, in-

Synthesis and properties of Me₄TACD

The commonly used method for preparing the Me₄TACD ligand consists of three steps. First, the Richman-Atkins cyclization assembles the macrocycle by reacting N,N',N"-tris(p-tolysulfonyl) diethylenetriamine-N,N"-disodium salt (A) with tosylbis[2-(tosyloxy)ethyl]amine (B) (Scheme 1).^{23,24} This cyclization can also be done using diethylamine B with mesyloxy or halides (Cl-I) as the leaving group.24 The highest yield of ~80% was obtained when the tosyloxy (OTs) group was used as a leaving group. 24 This cyclization works best when carried out in N,N-dimethylformamide. The second step is the detosylation of tetra(tosyl)cyclen using concentrated sulphuric acid. Finally, the N-methylation (Eschweiler-Clarke reaction) of the parent macrocycle H₄TACD employing a mixture of formic acid and formaldehyde provides Me₄TACD in 45-55% yield. ^{21,25} The main drawback of this route is its low atom economy, as it requires both tosylation and detosylation steps. Additionally, the cyclization step requires a large quantity of dry DMF. A more efficient alternative produces the parent cyclen in two steps with an overall yield up to 57% (route 2).26 The first step of this route involves the S-alkylation of dithiooxamide using excess bromoethane and subsequent reaction of the resulting bis-thioimido ester salt with triethylenetetraamine to afford the tricyclic bis-amidine (Scheme 1). The reduction of the bis-amidine with DIBALH in refluxing toluene, followed by treatment with NaF in water, resulted in the parent

expensive and non-toxic, reactions and catalysis based on molecularly defined complexes could eventually substitute some reactivity patterns so far dominated by transition metals.

^aDepartment of Chemistry, Indian Institute of Technology, Gandhinagar, Gujarat-382355, India

^bDepartment of Chemistry, University of Bath, Bath, BA2 7AY, UK

^cInstitute of Inorganic Chemistry, RWTH Aachen University, Landoltweg 1, 52056 Aachen, Germany. E-mail: jun.okuda@ac.rwth-aachen.de

Dalton Transactions Perspective

Route 1

Route 2

Scheme 1 Synthetic methods of the ligand Me₄TACD. (i) DMF, 100 °C. (ii) H₂SO₄ (conc.), NaOH. (iii) HCO₂H/CH₂O, 100 °C, NaOH. (iv) DIBAL-H, refluxing toluene. (v) NaF, H₂O.

cyclen. Finally, *N*-methylation of cyclen using the Eschweiler–Clarke reaction provides Me₄TACD. ^{21,25,26}

As a ligand, Me₄TACD generally binds to a metal fragment MLX in a κ^4 -fashion and adopts a C_4 -symmetric, boat-like conformation (Fig. 1a). The four nitrogen atoms of the ligand form a square planar core with the coordinated metal residing above the plane and all four NMe groups pointing towards the metal. In the solid state, the four CH₂CH₂ groups adopt a staggered conformation to avoid steric congestion, giving rise to two enantiomers ($\delta\delta\delta\delta$, $\lambda\lambda\lambda\lambda$) for an achiral metal center. The CH₂ protons of the ligand are magnetically inequivalent, leading to AA'XX'-type signal sets for CH₂CH₂ groups in the ¹H NMR spectrum. Depending on the size of the coordinated metal ion, lability of N–M bonds, and remaining coordination sphere, the AA'XX'-spin system can appear resolved, unresolved AB spin system, or collapsed broad singlet on the NMR time-

scale. AB-multiplets indicate rapid ring flipping between the two enantiomers but persistent macrocycle coordination with two disparate faces, whilst complete collapse can indicate fluxional ligand coordination. In two examples shown below, 27,28 the Me₄TACD ligand has been observed to adopt a folded conformation where one of the four methyl groups is orientated away from the metal centre (Fig. 1b). This highly strained conformation appears to relieve steric congestion for small metal cations with two strongly-bound ancillary X-type ligands (Al-H, Mg-O); weakly bound X-type ligands (e.g. Zn-I) are readily displaced by the chelating macrocycle to give auto-ionised products of the type $[(\kappa^4\text{-Me}_4\text{TACD})\text{MX}]^+\text{X}^-$. The folded conformation in solution is diagnosed with ¹H NMR spectroscopy by the presence of three methyl environments in a 1:2:1 integral ratio and 8-sets of magnetically inequivalent CH₂ protons in the ¹H NMR spectrum. ²⁸

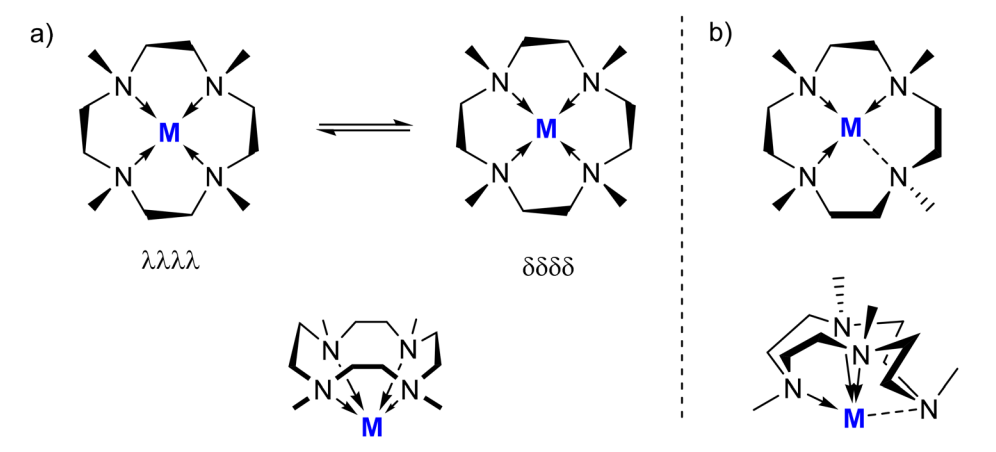


Fig. 1 Coordination behaviour of Me₄TACD ligand: (a) κ^4 NNNN-bonding with boat-like conformation; (b) κ^3 NNN-bonding with folded conformation.

Perspective **Dalton Transactions**

Group 1 metals

Alkali metal compounds typically exist as saline or aggregated species, but neutral polydentate ligands help to stabilize welldefined low-nuclearity molecular species. Polyamines offer advantages over crown-ethers due to stronger $N \rightarrow M$ bonds and being less prone to nucleophilic attacks. Indeed, large azacrowns have been used to stabilise highly reducing sodide compounds.29 A renewed interest in organoalkali compounds as useful reagents in synthetic organic chemistry 17,20,30 has highlighted the impact of different chelating donor ligands on reactivity and chemoselectivity. 18,19,31 While the use of Me,4TACD remains limited to the examples described herein, the steric and coordinative demand and strong chelate effect (especially for lithium and sodium) make it a promising candidate for the future development of organoalkali metal chemistry.

Trends in alkali metal coordination chemistry of Me₄TACD complexes depend on the ionic radius and strength of M-N bonds. While lithium forms strong, monomeric complexes with 12-membered aza-crown with appreciable covalency in Li-N bonds, the heavier alkali metals exhibit more labile bonding, leading to dimeric or polymeric structures. Me₄TACD has been employed to provide well-defined molecular hydridotriphenylborates, which were employed as catalysts in the hydroboration of unsaturated organic substrates. Low-nuclear-

Scheme 2 Equilibrium between the contact ion pair and the solventseparated ion pair of 1 in THF.

ity triphenyl- and trihydridosilanide complexes have also been structurally characterised.

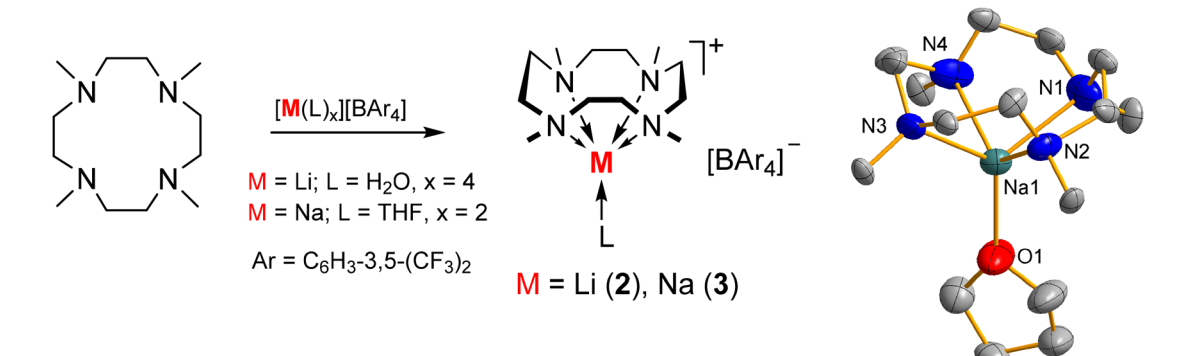
Charge-separated lithium and sodium complexes 3.1.

The lithium complex of Me₄TACD ligand, $[(Me_4TACD)^6Li][CH(C_6H_5)(S-C_6H_5)]$ (1), which was obtained upon treatment of [6Li]-α-(phenylthio)benzyllithium with one equiv. of Me₄TACD in THF/THF-d₈, was prepared to study its structure in solution by NMR spectroscopy.32 Based on 6Li-HOESY, 1H, and 13C NMR spectroscopy, the study revealed an equilibrium between contact ion pairs and solvent-separated ion pairs at ambient temperature and with an increased proportion of solvent-separated ion pairs at lower temperatures (Scheme 2).

Me₄TACD ligated lithium and sodium complexes $[(Me_4TACD)M(L)][BAr_4]$ (M = Li (2), Na (3); L = H₂O, THF; Ar = C_6H_3 -3,5-(CF_3)₂) were prepared from their respective borate salts $[Li(H_2O)_4][BAr_4]$ and $[Na(THF)_2][BAr_4]$ (Scheme 3). 33,34 Attempts to isolate the heavier homologues resulted in [(Me₄TACD)H][BAr₄], likely due to hydrolysis from traces of water present in the solvent. Unlike the sandwich structure of [12]-crown-4 complexes of group 1 metals, these complexes exhibit half-sandwich structures with five-coordinate alkali metal cations of square pyramidal geometry (Scheme 3). The Me₄TACD ligand adopts a distorted boat-like conformation, positioning all four nitrogen atoms in a square planar arrangement. The metal cations are located below this N₄ plane, with all NMe groups oriented toward the metal centre. In solution, the Me₄TACD ligand binds the alkali metals more strongly than the corresponding crown ethers, as evidenced by a significant downfield shift of the 23 Na NMR signal (δ (23 Na) +12.7 ppm (3) vs. ~0 ppm for $[Na([12]-crown-4)_2]^+)$.³³ In fact, the coordination of alkali metals to the aza-macrocycle is not just an electrostatic interaction but also involves a significant donation of electron density from the nitrogen's 2p-nonbonding orbitals to the alkali metal center.34

3.2. Alkali metal hydridotriphenylborates

Me₄TACD-supported alkali metal hydridotriphenylborates $[(Me_4TACD)M][HBPh_3]$ (M = Li (4), Na (5), K (6)) were syn-



Scheme 3 Synthesis of the Li and Na borate complexes of Me₄TACD; molecular structure of the cationic part of 3.

Dalton Transactions Perspective

$$[M\{N(SiHMe_2)_2\}] \begin{tabular}{ll} \hline Me_4TACD & $[(Me_4TACD)M\{N(SiHMe_2)_2\}]$ & N_3 & N_4 & N_1 & N_2 & N_3 & N_3 & N_2 & N_3 &$$

Scheme 4 Synthesis of Me₄TACD ligated alkali metal hydridotriphenylborates and the molecular structure of 6.

thesized via two pathways.³⁵ One approach involves a two-step, one-pot reaction where Me₄TACD reacts with tetramethyldisilazides $[M{N(SiHMe_2)_2}]$ (M = Li, Na, K) in THF, followed by BPh₃ to obtain compounds 4-6 after elimination of (Me₂HSiN-SiMe₂)₂ (Scheme 4). The other method involves mixing Me4TACD with the alkali metal hydridotriphenylborates [M(HBPh3)] in THF (Scheme 4, left). The structural analysis of 4-6 revealed distinct bonding geometries: while the lithium complex 4 forms a separated ion pair with a THF molecule at the lithium, the sodium (5) and the potassium (6) homologues exist as contact ion pairs due to the non-covalent $M^+ \cdots C_{\pi}$ (M = Na, K) interactions along with a 3-centered-2-electron M···H-B bonding interaction (Scheme 4). The five-coordinate lithium cation in compound 4 adopts a distorted squarepyramidal geometry. For compounds 5 and 6, the sodium and the potassium cations are formally eight and nine coordinated and exist in a distorted square anti-prismatic and monosquare anti-prismatic geometry, capped respectively. Compounds 4-6 serve as chemoselective catalysts for carbonyls and CO₂ hydroboration, with the lithium complex exhibiting the highest activity.35 While the hydridoborate provides the hydride in catalysis, the alkali metals and supporting ligand play an important role in activating the substrate by its Lewisacidic properties. Lower denticity acyclic polyamines N,N,N',N'tetramethylethylenediamine (TMEDA) and N,N,N',N",N"-pentamethyldiethylenetriamine (PMDTA) provide higher activity than Me₄TACD derivatives due to easier access to the metal centre. The tetradentate, yet hemilabile ligand N,N,N',N',N'',N'',N''hexamethyltriethylenetetraamine (Me6TREN) provided further improved activity.36

3.3. Alkali metal silanides

Given the current interest in hydrogen storage materials, the alkali metal silanides $[MSiH_3]_{\infty}$ (M = Li–Cs) have been widely studied recently.^{37–40} Normally, alkali metal silanides are thermodynamically unstable and exist as polymeric clusters. Employing the Me₄TACD ligand, a series of molecular alkali metal silanides $[(Me_4TACD)M(SiH_3)]_n$ (M = Li (12), Na (13), K

(14) and Rb (15); n = 1-2) were isolated, and exist as monomer or dimer in the solid-state. 41 Compounds 12-15 were prepared from triphenylsilanides $[(Me_4TACD)M(SiPh_3)]_n$ (M = Li (7), Na (8), K (9a), Rb (10); n = 1 (Li-K), 2 (Rb)) and H₂ or PhSiH₃ (Scheme 5). Hydrogenolysis or hydrosilylation is chemoselective for the Si-C bonds to eliminate benzene or diphenylsilane, rather than heterolyzing the M-Si bond to provide the corresponding alkali metal hydride and hydrosilane. While the hydrogenolysis of 7-10 with H₂ takes several days to complete, the reaction with PhSiH₃ finishes within 5 min and proceeds with redistribution of the organosilane to give Ph2SiH2 and SiH₄. The triphenylsilanides 7-10, along with the caesium analogue [(Me₄TACD)Cs(SiPh₃)]_∞ (11), were synthesized from the reaction of Me₄TACD, Ph₃SiSiMe₃, and LiCH₂SiMe₃ or MO^tBu (M = Na-Cs). Alternatively, compounds 7 and 9-10 were prepared through the ligand exchange reaction from isolated THF adducts $[M(SiPh_3)(thf)_n]$ with Me₄TACD. Lithium (7) and sodium (8) triphenylsilanides exist as monomers with a direct M-Si σ-bond. The potassium complex was crystallised as a monomeric THF-adduct, [(Me4TACD)K(SiPh3)(thf)] (9b), which contains a K-Si σ-bond, but rapidly loses THF under vacuum to provide 9a, where the silanide is alternatively bound to potassium νia an η^6 - π -facial interaction. The stability of the triphenylsilanides decreases down the group (Li: $t_{1/2}$ = 14 d; Cs: $t_{1/2} \approx 12$ h). In contrast, the trihydridosilanide **12–15** shows a reverse trend; the Na, K, and Rb homologues are stable for weeks both in solution and solid state, but the Li homologue decomposes in two days. While the light alkali metal analogues 7-9 exist as a monomer in the solid state, the heavier analogues show a more extended coordination sphere (10: dimer with bridging [SiPh₃]; 11: one-dimensional chain-like structure through Cs-C_{Ph} interactions). Similarly, trihydridosilanide 13 exists in monomeric form with square pyramidal coordination geometry around the sodium atom. The potassium (14) and rubidium (15) homologues form dimers in the solid state, with SiH_3 anions bridging the two [(Me₄TACD)M] fragments.

The complete series of alkali metal triphenylsilanide derivatives enabled comparative NMR spectroscopic analysis of the

Ph₃Si-SiMe₃ LiCH₂SiMe₃ or MOtBu (Me₃Si)₂CH₂ H_2 (1 bar) or tBuOSiMe3 or PhSiH₃ M = Na - Cs $[(Me_4TACD)MSiPh_3(thf)_x]_n$ [(Me₄TACD)MSiH₃]_n __3 C₆H₆ or 7 (M = Li, n = 1, x = 0) **12** (M = Li, n = unknown) [(thf)_nMSiPh₃] - Ph₂SiH₂ SiH₄ 8 (M = Na, n = 1, x = 0) **13** (M = Na, n = 1) M = Li, K, Rb, Cs **9a** (M = K, n = 1, x = 0)**14** (M = K, n = 2)-THF **15** (M = Rb, n = 2)**9b** (M = K, n = 1, x = 1)**10** (M = Rb, n = 2, x = 0) **11** (M = Cs, n = ∞ , x = 0) Si1 Si1

Scheme 5 Synthesis of Me₄TACD stabilized alkali metal silanides (top) and molecular structure of potassium silanide complexes 9a and 14.

binding of the Me_4TACD ligand to metal cations with increasing ionic radius. The lithium (7) and sodium (8) complexes show two multiplets for the methylene protons in their 1H NMR spectrum (THF- d_8 , 25 $^{\circ}C$), consistent with time-averaged C_{4v} -symmetry and persistent ligand coordination. In contrast, compounds 9–11 show a broad signal for the methylene environment, which is also notably sharper for Cs (11) than for K (10), indicating increasingly faster ligand dynamics for the larger metal cations. The similarity of the methylene chemical shift (δ 2.4 ppm) to that of the free ligand suggests partial ligand dissociation.

3.4. Molecular alkali metal organoperoxides

Alkali metal organoperoxides [MOOR] (M = Li, Na, K; R = hydrocarbyl), which form as unstable intermediates in the oxidation of organometallics by O₂, exist in oligomeric forms. The Me₄TACD ligand is suitable for stabilizing such highly reactive peroxide intermediates. The addition of Me₄TACD to an *n*-pentane solution of LiNⁱPr₂ and ROOH (R = ^tBu, CMe₂Ph) at ambient temperature and subsequent cooling gave the molecular organoperoxides [(Me₄TACD)Li(OOR)(ROOH)] [R = ^tBu (16), CMe₂Ph (17)] (Fig. 2, left). The same reactions without the Me₄TACD ligand gave the dodecameric clusters [LiOOR]₁₂. When Me₄TACD was treated with [MN(SiMe₃)₂] (M = Na, K) and ^tBuOOH in a 1:1:5 ratio in *n*-pentane, corresponding molecular organoperoxides [(Me₄TACD)M(OO^tBu)(^tBuOOH)₃]

Fig. 2 Light alkali metal organoperoxides stabilized by Me₄TACD.

(M = Na (18), K (19); Fig. 2, right) were obtained in good yields. In all the syntheses, an excess of organoperoxides was necessary to maintain the homogeneity of the reaction mixtures. Single-crystal X-ray diffraction studies confirmed the mononuclear nature of compounds 17, 18, and 19, with lithium in a hexa-coordinate environment, while sodium and potassium adopt an eight-coordinate, distorted square-antiprismatic geometry. The O-H···O hydrogen bonding between the metal-coordinated organoperoxides and neutral peroxides plays an important role in the stability of the complexes.

4. Group 2 metals

The Me₄TACD ligand was utilized to stabilize molecular hydrides of group 2 metals, suppressing aggregation into saline MH₂.

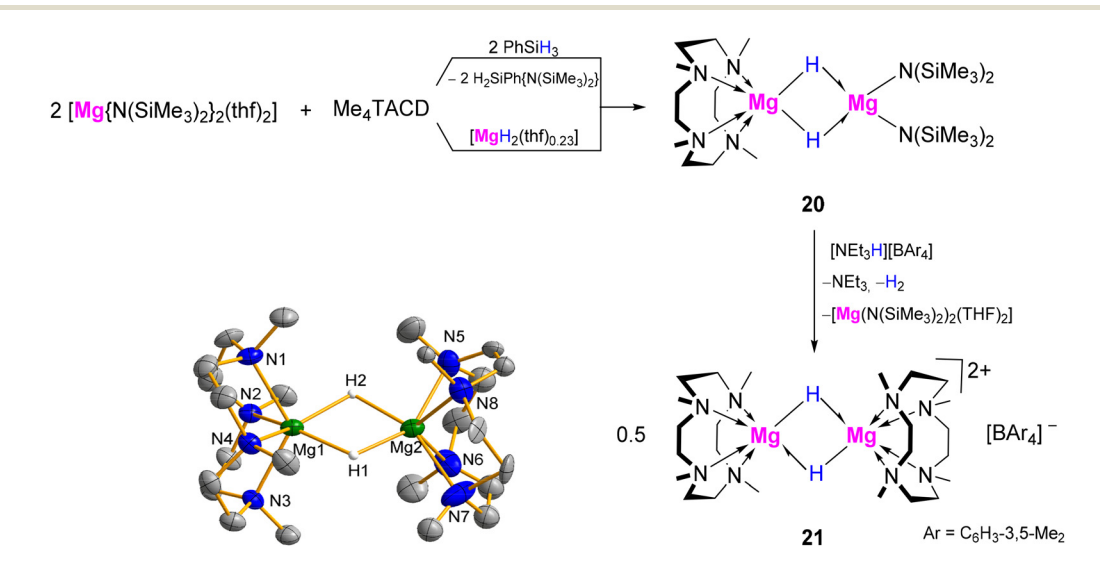
Dalton Transactions Perspective

Hydride complexes were synthesised via hydrogenolysis or hydrosilanolysis of organo- and silanido-alkaline earth precursors. Structural trends reflect decreasing electronegativity and increasing ionic radius and polarizability, with increasing atomic number. While discrete dimeric (di)cations [(Me₄TACD) $M_2H_n^{(4-n)+}$ (n = 2, 3) were structurally characterised for M = Mg, Ca, Ba, only a trimeric [(Me₄TACD)₃Sr₃H₄(thf)]²⁺ cluster was isolated for the Sr²⁺ ion. [(Me₄TACD)Mg₂H₂]²⁺ exhibits hydridic reactivity towards Lewis-acidic and polar unsaturated small molecules. The larger calcium congener can access a coordinatively unsaturated state; combined with highly nucleophilic hydride ligands, this enables H/D exchange under D₂ and catalytic hydrogenation/hydrosilylation of unactivated *n*-alkenes. The extreme nucleophilicity of Sr-H bonds led to the isolation of a rare hexahydridosilicate complex. Calcium and strontium hydrides are highly labile and undergo dynamic hydrideexchange equilibria. Neutral and cationic allyl, benzyl, and silyl derivatives of calcium, strontium, and barium have also been described as molecular Me₄TACD complexes. The Me₄TACD ligand has also used to stabilize related dinuclear polyhydride complexes of lanthanides, including vttrium, vtterbium and lutetium, highlighting its broad application in molecular hydride chemistry.44-46

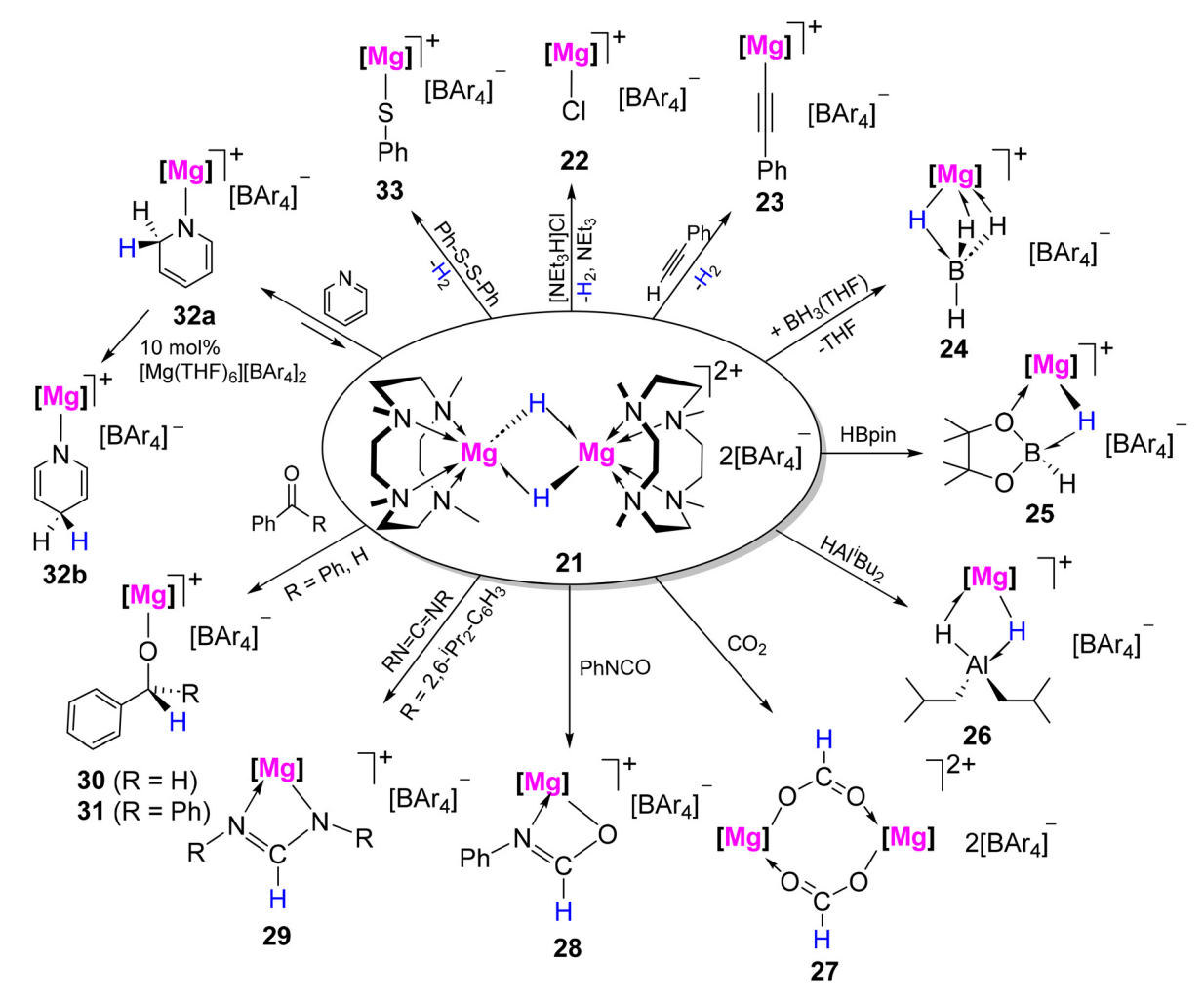
4.1. Magnesium

4.1.1. Synthesis of molecular magnesium hydride complexes. The neutral magnesium hydride [(Me₄TACD)Mg(µ- $H_2Mg\{N(SiMe_3)_2\}_2$ (20) was synthesized in 82% yield by reacting a mixture of [Mg{N(SiMe₃)₂}₂(thf)₂] and Me₄TACD with PhSiH₃ in aromatic solvents (Scheme 6).⁴⁷ Alternatively, compound 20 was also obtained directly by reacting magnesium dihydride $[MgH_2(thf)_{0.23}]$ with $[Mg\{N(SiMe_3)_2\}_2(thf)_2]$ and Me₄TACD, but in lower yield (54%). The dinuclear structure of 20 observed in the solid state can be viewed as a monomeric [(Me₄TACD)MgH₂] stabilized by magnesium bis(amide) [Mg{N (SiMe₃)₂}₂]. The ¹H NMR spectrum in THF-d₈ showed a characteristic MgH resonance at δ 3.61 ppm. Partial protonolysis of 20 with $[NEt_3H][B(C_6H_3-3,5-Me_2)_4]$ afforded the cationic magnesium hydride $[(Me_4TACD)Mg(\mu-H)]_2[B(C_6H_3-3,5-Me_2)_4]_2$ (21) in 43% yield after elimination of H2, NEt3, and [Mg{N $(SiMe_3)_2$ (Scheme 6). The deuterium analogue of $[(Me_4TACD)_2Mg_2(\mu-D)_2][B(C_6H_3-3,5-Me_2)_4]_2$ (21-d₂) was synthesized using PhSiD₃ or in an exchange reaction of 21 with D₂ over 54 h. In the D_{2h} -symmetric structure of 21, two macrocyclic ligands bind the $[Mg_2(\mu-H)_2]^{2+}$ core in a κ^4 -coordination mode and in a staggered conformation, which differs from the eclipsed conformation observed in its calcium analogue 42a.

4.1.2. Reactivity of molecular magnesium hydride complexes. Hydridic nature of the Mg-H functionality in 21 was exploited in the reaction with the weak Brønsted acids [NEt3H] Cl and PhC≡CH, affording the monomeric magnesium complexes $[(Me_4TACD)MgX][B(C_6H_3-3,5-Me_2)_4](X = Cl(22), C = CPh$ (23)) (Scheme 7).48 Lewis acids, such as BH3(thf), HBpin and DIBAL(H) gave the hydride-bridged mononuclear adducts $[(Me_4TACD)Mg(\mu-H)_3BH][B(C_6H_3-3,5-Me_2)_4]$ (24), $[(Me_4TACD)$ $Mg(\mu-H)BHpin [B(C_6H_3-3,5-Me_2)_4]$ (25) and $[(Me_4TACD)Mg(\mu H_{2}Al^{i}Bu_{2}[B(C_{6}H_{3}-3,5-Me_{2})_{4}]$ (26), respectively (Scheme 7).⁴⁷ While insertion of CO₂ into the Mg-H bond gave the dimeric $[(Me_4TACD)_2Mg_2(\mu-O_2CH)_2][B(C_6H_3-3,5$ formate complex $Me_2)_4$ ₂ (27), the reactions with PhN=C=O and (Dipp) N=C=N(Dipp) (Dipp = 2,6- $^{i}Pr_{2}-C_{6}H_{3}$) afforded the monomeric compounds $[(Me_4TACD)Mg(OCHNPh)][B(C_6H_3-3,5-Me_2)_4]$ (28) $[(Me_4TACD)Mg\{(DippN)_2-CH\}_2][B(C_6H_3-3,5-Me_2)_4]$ (29), respectively (Scheme 7).48 Similarly, benzaldehyde and benzophenone both insert into the Mg-H bond to afford the monomeric alkoxides [(Me₄TACD)Mg(OCH(R)Ph)][B(C₆H₃-3,5-Me₂)₄] (R = Me (30); Ph (31)). 47 Magnesium hydride 21 also reduces pyridine to give the 1,2-dihydridopyridyl (DHP) complex $[(Me_4TACD)Mg(1,2-DHP)][B(C_6H_3-3,5-Me_2)_4]$ (32a; Fig. 3),



Scheme 6 Me₄TACD-supported magnesium hydrides 20 and 21 and the molecular structure of the dicationic part of 21. Ar = C₆H₃-3,5-Me₂.



Scheme 7 Reactivity of magnesium hydride 21; $[Mg] = [(Me_4TCD)Mg]^{2+}$; Ar = C_6H_3 -3,5- Me_2 -

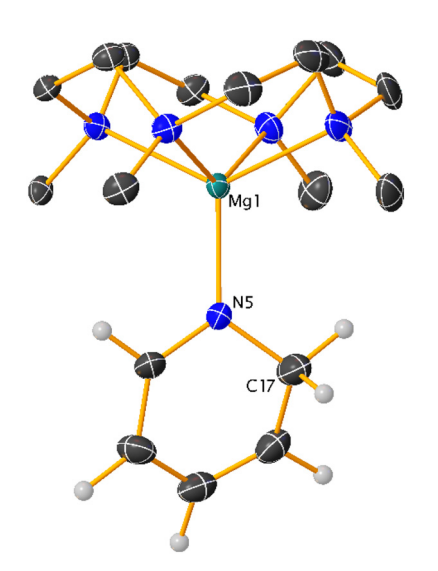


Fig. 3 Molecular structure of the cationic part of 1,2-dihydropyridyl complex 32a.47

which isomerises to the 1,4-dihyridopyridyl $[(Me_4TACD)Mg(1,4-DHP)][B(C_6H_3-3,5-Me_2)_4]$ (32b) in the presence of catalytic amount of [Mg(thf)₆][B(C₆H₃-3,5- $Me_2)_4]_2.^{47}$

Dihydridopyridyl complexes 32a and 32b undergo slow exchange with pyridine- d_5 at 70 °C to give fully deuterated species 32a-d₆ and 32b-d₆ via partially deuterated species 32a d_5 and 32b- d_5 . Due to the reversibility of the 1,2-insertion, gradual generation of the deuteride 21-d accounts for the fully deuterated species. Compounds 32a and 32b catalysed the hydroboration of pyridine using pinacolborane, providing a mixture of regioisomers. 47 Compound 21 reacts with diphenyl disulfide to give the thiophenolate complex [(Me₄TACD)Mg $(SPh)[B(C_6H_3-3,5-Me_2)_4]$ (33) after H₂ elimination.⁴⁸

The dimeric formate complex 27 crystallized as a co-crystalline mixture of two conformers. The minor conformer displayed a rare folded conformation of the Me₄TACD ligands (Fig. 1b), with one of the NMe groups pointing away from the metal.48 However, according to NMR spectroscopy, the ligand in solution adopts its usual C4-symmetric, boat-like conformation.

Dalton Transactions Perspective

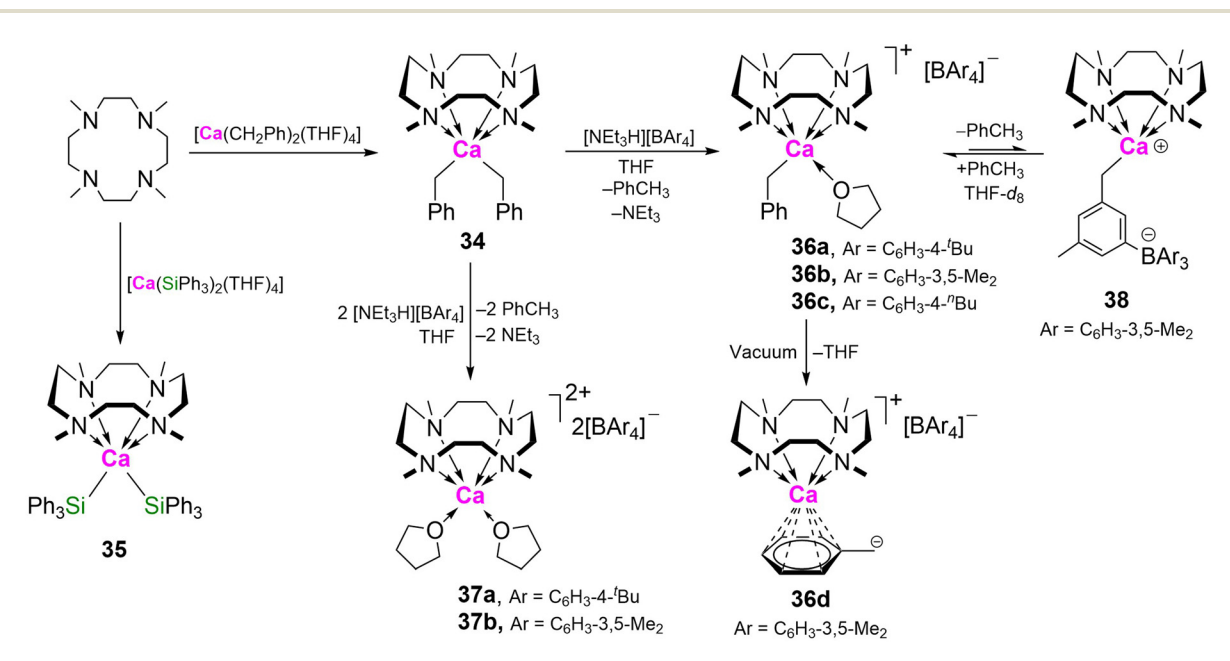
4.2. Calcium

4.2.1. Organo- and silanido-calcium complexes. Neutral dibenzyland bis(triphenylsilyl)calcium complexes $[(Me_4TACD)Ca(CH_2Ph)_2]$ (34) and $[(Me_4TACD)Ca(SiPh_3)_2]$ (35) were synthesised by treating THF solutions of the corresponding THF-solvates $[Ca(CH_2Ph)_2(thf)_4]$ (SiPh₃)₂(thf)₂] with Me₄TACD (Scheme 8). 49,50 The orange dibenzyl complex is insoluble in THF and precipitates directly from the reaction mixture, whilst the bis(silvl) derivative is somewhat soluble in this solvent and was precipitated from a THF/n-pentane mixture. Single crystals of 34 were grown by layering THF solutions of [Ca(CH₂Ph)₂(thf)₄] and Me₄TACD.⁴⁹ The six-coordinate metal centre adopts a distorted trigonal prismatic geometry with each benzyl ligand bound in an η^1 manner through the formally sp³-hybridised carbanionic methylene carbon. The Ca-C(1) distances (2.6392(19) Å) are significantly longer than those of the tetrakis(THF)-solvate (2.568(5)-2.595(5) Å).⁵¹ The crystal structure of vellow [(Me₄TACD)Ca(SiPh₃)₂] similarly adopts a distorted trigonal prismatic geometry, with a Ca-Si distance (3.1654(15) Å) comparable to that of the precursor.⁵⁰

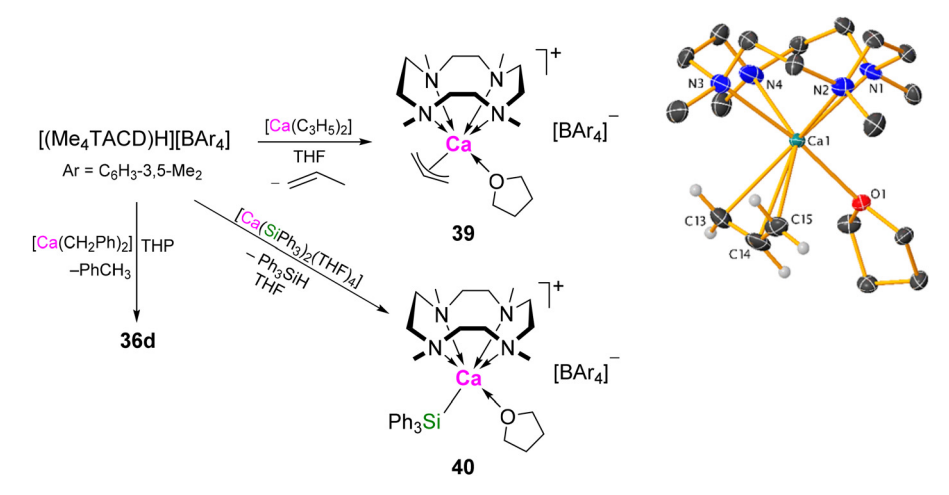
Dibenzyl 34 reacts with the weak Brønsted acid $[NEt_3H][BAr_4]$ (Ar = C₆H₄-4-^tBu, C₆H₃-3,5-Me₂, C₆H₄-4-ⁿBu) to yield the cationic benzyl complex [(Me₄TACD)Ca(CH₂Ph) (thf)][BAr₄] (36a, Ar = C_6H_4 -4-^tBu; 36b, Ar = C_6H_3 -3,5-Me₂; 36c, Ar = C_6H_4 -4-ⁿBu) (Scheme 8). Loss of THF provides access to the \(\eta^6\)-benzyl complex \[\left[(Me_4TACD)Ca(CH_2Ph) \right] \[B(C_6H_3-3,5-1) \] Me₂)₄] (36d).⁴² The related red ytterbium(II) analogues $[(Me_4TACD)Yb(CH_2Ph)_2]$ (34-Yb) and $[(Me_4TACD)Yb(CH_2Ph)][B$ (C₆H₃-3,5-Me₂)₄] (36d-Yb) have also been synthesised and crystallographically characterised; similar to calcium, both benzyl moieties are η¹-bonded for 34-Yb, but purple 36d-Yb crystallises as an n⁶-benzyl complex without coordinated THF.⁴⁴ Addition of two equiv. of [NEt₃H][BAr₄] to 34 provided the dicationic bis(borate) salt [(Me₄TACD)Ca(thf)₂][BAr₄] (37a, Ar = $C_6H_4-4^{-t}Bu;^{49}$ 37b, Ar = $C_6H_3-3,5-Me_2$).⁵² In THF-solution, 36b was found to exist in equilibrium with the zwitterionic compound $[(Me_4TACD)Ca\{CH_2(C_6H_3-3-BAr_3-5-Me)\}]$ (38, Ar = C_6H_3 -3,5-Me₂) via deprotonation of one of the meta-methyl groups of the borate anion and elimination of toluene. 49 Notably, in contrast to 34, the putative neutral dibenzyl complex of the pentadentate aza-macrocycle Me₅PACP (Me₅PACP = N,N',N",N"',N"' "-pentamethyl-1,4,7,10,13-pentaazacyclopentadecane" unstable to ligand decomposition.53

Cationic calcium derivatives can be accessed by protonolysis of neutral bis(organo)calcium or bis(silanido)calcium precursors using cationic conjugate acid of Me4TACD (Scheme 9). $^{42,53-55}$ Reaction of $[(Me_4TACD)H][B(C_6H_3-3,5-1)]$ Me₂)₄] with a THP slurry of THF-free dibenzylcalcium [Ca (CH₂Ph)₂], provided direct access to the η⁶-benzyl complex 36d. 42 Similarly, bis(allyl)calcium reacts with [(Me₄TACD)H][B $(C_6H_3-3,5-Me_2)_4$ in THF to yield the cationic allyl complex $[(Me_4TACD)Ca(\eta^3-C_3H_5)(thf)][B(C_6H_3-3,5-Me_2)_4]$ (39) under elimination of propene.⁵⁴ 39 adopts a distorted pseudo-trigonal prismatic geometry with the allyl ligand coordinating in an η³-manner. Protonolysis of bis(triphenylsilanido)calcium with $[(Me_4TACD)H][B(C_6H_3-3,5-Me_2)_4]$ yielded a cationic silanide complex, 40, characterised by NMR spectroscopy. 42

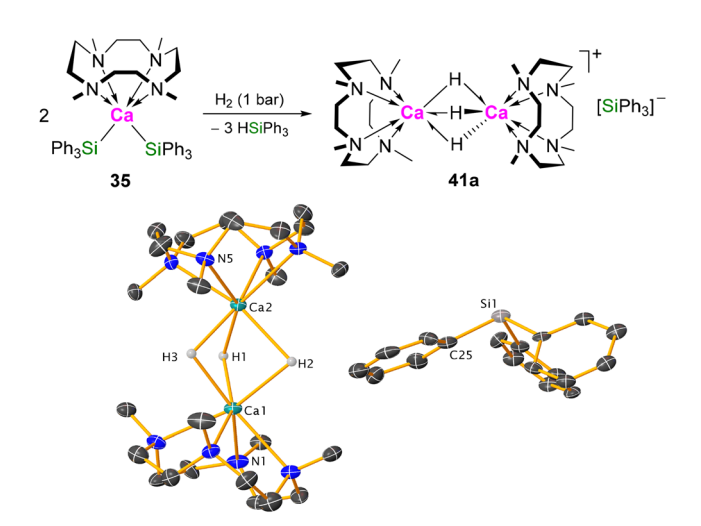
4.2.2. Synthesis of molecular calcium hydride complexes. Unlike alkali metal triphenylsilanides 7-11, which form parent silanides 12-15 upon hydrogenolysis, (Scheme 5)41 35 reacts with H₂ by heterolysis across the Ca-Si bonds to provide a dimeric trihydride cation as its charge-separated triphenylsilanide salt [(Me₄TACD)₂Ca₂(μ-H)₃][SiPh₃] (41a) and triphenylsilane (Scheme 10).50 Closely related Yb(II) silanide complex



Scheme 8 Synthesis of Me₄TACD ligated calcium benzyl and silanide complexes 34-38



Scheme 9 Direct access to cationic calcium η^6 -benzyl (36d), η^3 -allyl (39), and triphenylsilanide (40) complexes by protonolysis using [(Me₄TACD) H][BAr₄]. The cationic part of the crystal structure of compound 39.



Scheme 10 Hydrogenolysis of compound 35 and molecular structure of dicalcium trihydride silanide salt 41a.

[(Me₄TACD)Yb(SiPh₃)₂] is similarly hydrogenated to provide the congeneric black Yb(π) trihydride dimer [(Me₄TACD)₂Yb₂(μ -H)₃[SiPh₃].⁴⁴

Hydrogenolysis of **34** provided an insoluble precipitate, likely CaH_2 , along with free Me_4TACD and decomposition products. However, using triphenylsilane as a hydride source produced a dimeric dicalcium dihydride cation, which crystallised as its triphenylsilylbenzyl salt $[(Me_4TACD)_2Ca_2(\mu H)_2][PhCHSiPh_3]_2$ (**42a**) (Scheme 11). ⁴⁹ The crystal structure of **42a** consists of a dicationic C_i -symmetric dimer with two six-coordinate calcium centres bridged by two μ -hydride ligands. **42a** decomposes in THF- d_8 ($t_{1/2} = 6$ h) via ligand degradation with formation of PhCH₂SiPh₃ amongst other species. Due to the reactive silylbenzyl anion, **42a** activates H_2 in an FLP-like manner to yield the dimeric trihydride cation $[(Me_4TACD)_2Ca_2(\mu-H)_3][PhCHSiPh_3]$ (**41b**) under elimination of

 $PhCH_2SiPh_3$. **41b** can also be formed directly by hydrogenolysis of **34** in the presence of $PhCH_2SiPh_3$.

Molecular calcium di- and trihydride dimers can be accessed as relatively robust tetraarylborate salts via hydrogenolysis of 36 or a 1:1 mixture of 36 and 34 (Scheme 12), respectively providing $[(Me_4TACD)Ca_2(\mu-H)_2][BAr_4]_2$ (42b, Ar = C_6H_4 -4- tBu ; 42c, Ar = C_6H_3 -3,5-Me₂) or $[(Me_4TACD)Ca_2(\mu-H)_3][BAr_4]$ (41c, Ar = C_6H_4 -4- tBu ; 41d, Ar = C_6H_3 -3,5-Me₂). ⁴⁹ 41c can be converted to 42c via protonolysis by addition of $[NEt_3H][B(C_6H_4$ -4- $^tBu)_4]$, or through hydride-redistribution by combining with calcium bis(borate) 37a. Hydrogenolysis of 36 42,53 or silanolysis of either 36 42,53 or 39 54 with RSiH₃ (R = n-octyl or Ph), followed by crystallisation from THF/n-pentane provides reliable access to the dimeric dihydride dication as a THF-solvate $[(Me_4TACD)_2Ca_2(\mu-H)_2(thf)][BAr_4]_2$ (42d, Ar = C_6H_3 -3,5-Me₂; ⁵⁴ 42e, Ar = C_6H_3 -4- nBu). ⁵³

The crystal structures of **42d** (Fig. 4),⁵⁴ and **42e** ⁵³ reveal a dimeric dication with six- and seven-coordinate calcium centres bridged by two μ -hydrides. Compared to **42a**, the seven-coordinate calcium centre exhibits longer Ca–H distances, leading to an elongated Ca–Ca separation (3.6306(11) Å ν s. 3.4650(10) Å). The red Yb(II) congener [(Me₄TACD)₂Yb₂(μ -H)₂(thf)][B(C₆H₃-3,5-Me₂)₄]₂ is isostructural to **42d**, and was prepared similarly by hydrogenolysis of the corresponding cationic Yb(II) benzyl complex.⁴⁴

In THF- d_8 solution, the anions have minimal effect on the hydride resonances of trihydride complexes **41a–d**, with silanide, silylbenzyl, and tetraarylborate salts all displaying a singlet at δ 4.71–4.73 ppm in their ¹H NMR spectra. ^{49,50} However, the dihydride silylbenzyl salt **42a** exhibits a significantly downfield-shifted hydride resonance (δ 4.70 ppm) ⁴⁹ compared to borate salts **42b–e** (δ 4.49–4.54 ppm). ^{42,49,53,54} This indicates that whilst compounds **41a–d** and **42b–e** exist as charge-separated species in THF, a significant anion–cation interaction may exist for **42a**. THF coordination to the dicationic core in **42** is highly labile, as **42c** and **42d** exhibit identical

Scheme 11 Synthesis of dicalcium di- and trihydrides 42a and 41b via hydrogenolysis and silanolysis of benzyl precursors in THF. Molecular structure of compound 42a with selected hydrogen atoms shown.

NMR spectra with time-averaged C_i -symmetry, and THF resonates at the same shift as free solvent. Coordination of THF to the unsolvated dimer $[(Me_4TACD)_2Ca_2H_2]^{2+}$ is mildly exothermic (ca. 33 kJ mol⁻¹),⁵⁴ consistent with Lewis acidity of the relatively large and coordinatively unsaturated metal cation.

Molecular calcium hydrides commonly adopt a dimeric dihydride structure when supported by bulky or highly coordinating ligands to suppress further aggregation. The dimeric trihydride motif $[(L)_2M_2H_3]^{\scriptscriptstyle +}$, however, is unique in alkalineearth chemistry to cationic complexes supported by neutral macrocycles, observed only in compounds 41a-d and the related strontium hydride $[(Me_5PACP)_2Sr_2(\mu\text{-}H)_3][B(C_6H_3\text{-}3,5\text{-}Me_2)_4].^{52}$ The ability to accept a third hydride reflects the electrophilic and coordinatively unsaturated nature of the metal cations in the dimeric dihydride. The combination of nucleophilic hydride and electrophilic metal centre is crucial to the

observed reactivity of such complexes towards kinetically inert substrates such as ethylene and carbon monoxide (vida~infra), and in the catalytic hydrogenation and hydrosilylation of olefins. The kinetic stabilisation of low-nuclearity calcium hydrides is dependent on ligand bulk and coordination strength. Employing the smaller Me₃TACN (N,N',N''-trimethyl-1,4,7-triazacyclononane) ligand results in the isolation of tetranuclear [(Me₃TACN)₄Ca₄(μ -H)₆][B(C₆H₃-3,5-Me₂)₄]₂.⁵⁵ Discrete calcium hydride clusters can be isolated via silanolysis of amide precursors. ^{56,57} Cluster nuclearity can be controlled by the size of supporting amine and/or amide ligands, with smaller clusters exhibiting higher activity as hydrogenation catalysts. ^{58,59}

4.2.3. Reactivity of molecular calcium hydride complexes

Dihydrogen and hydrosilanes. The silanide salt of dicalcium trihydride 41a exchanges with D_2 forming 41a- d_3 and HD via mixed isotopomers (Scheme 13). This was proposed to involve

36b,c (R = CH₂Ph) **Scheme 12** Synthesis of dimeric calcium hydrides **41c,d**, and **42b-e** in THF.

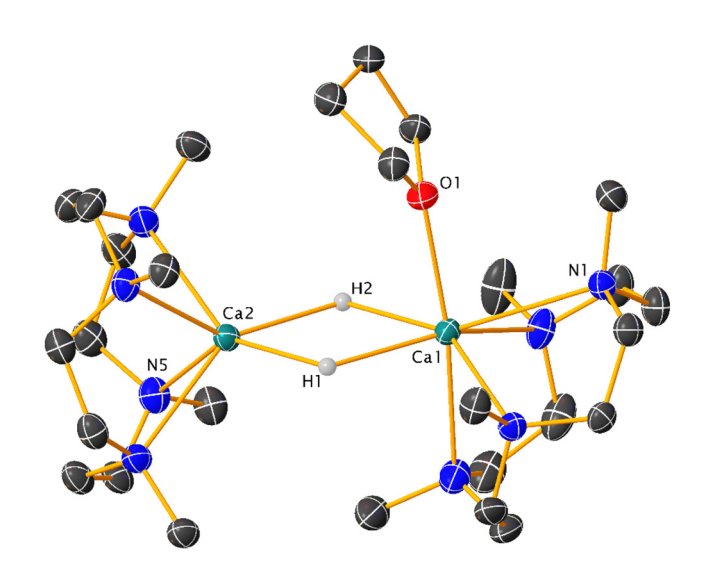


Fig. 4 Molecular structure of the dicationic part of compound 42d.

the silyl anion, as carrying out the reaction with D_2 in the presence of $HSiPh_3$ also resulted in H/D exchange to give $DSiPh_3$. Dimer-dissociation is implied by the rapid equilibration of **41a** and **41a**- d_3 to a mixture of isotopomers.⁵⁰ **42b** also exchanges

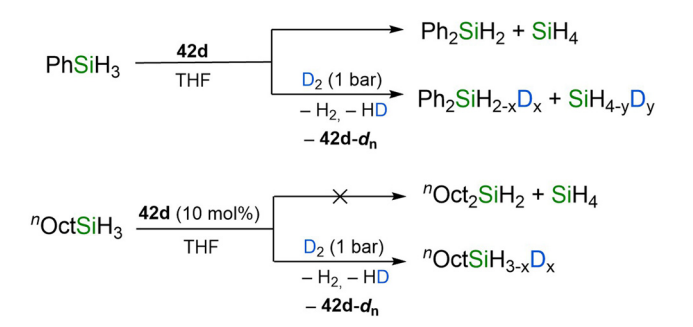
with D_2 ; formation of HD was observed by NMR spectroscopy, and complete deuteration occurred after 8 h (1 bar pressure), via intermediate formation of the monodeutero isotopomer (Scheme 13). Exposing **42b** to an equimolar mixture of D_2 and H_2 or HD resulted in rapid equilibration to a mixture of isotopomers after 5 min with respective formation of HD or H_2 and D_2 .

42d catalyses organosilane redistribution, converting PhSiH₃ into Ph₂SiH₂ and SiH₄ (Scheme 14). Exposing a solution of 42d and RSiH₃ (R = n-octyl, Ph) to D₂ produces HD, **42d**- d_n , and an isotopomeric mixture of hydrosilanes.⁵⁴ Broad SiH and CaH resonances in the ¹H NMR spectrum suggest mutual exchange according to EXSY NMR experiments, while NOESY NMR reveals NOE correlations between the silicon hydrides and NCH3 resonances. The reaction likely involves hypervalent silicates formed via nucleophilic hydride attack on silane. Similar propositions have been made for [(BDI^{dipp})Ca $(\mu-H)_{2}$ (BDI^{dipp} = HC{C(CH₃)N(C₆H₃-2,6-ⁱPr₂)}₂) synthesis using PhSiH₃ as a hydride source.³ Hypervalent silicates have been experimentally and computationally implicated as intermediates in alkaline-earth catalysed Si-E dehydrocoupling (E = N, O) reactions, in preference to concerted σ -bond metathesis. 60-62 Further, crystallographically characterised calcium and strontium hydridosilicate complexes derived from

Dalton Transactions Perspective

$$\begin{array}{c} Ph_{3}SiH \\ D_{2} \ (1 \ bar) \\ -HD \end{array} \begin{array}{c} Ph_{3}SiD + \textbf{41a-d_{3}} \\ -HD \end{array} \\ \hline Ph_{3}SiD + \textbf{41a-d_{3}} \\ \hline Ph_{3}SiD + \textbf{41$$

Scheme 13 Isotopic exchange of 41a and 42b.



Scheme 14 Calcium-mediated redistribution and deuteration of organosilanes.

the reaction of organo- and amido-alkaline earth complexes with hydrosilanes have also been isolated (vide infra). 63,64

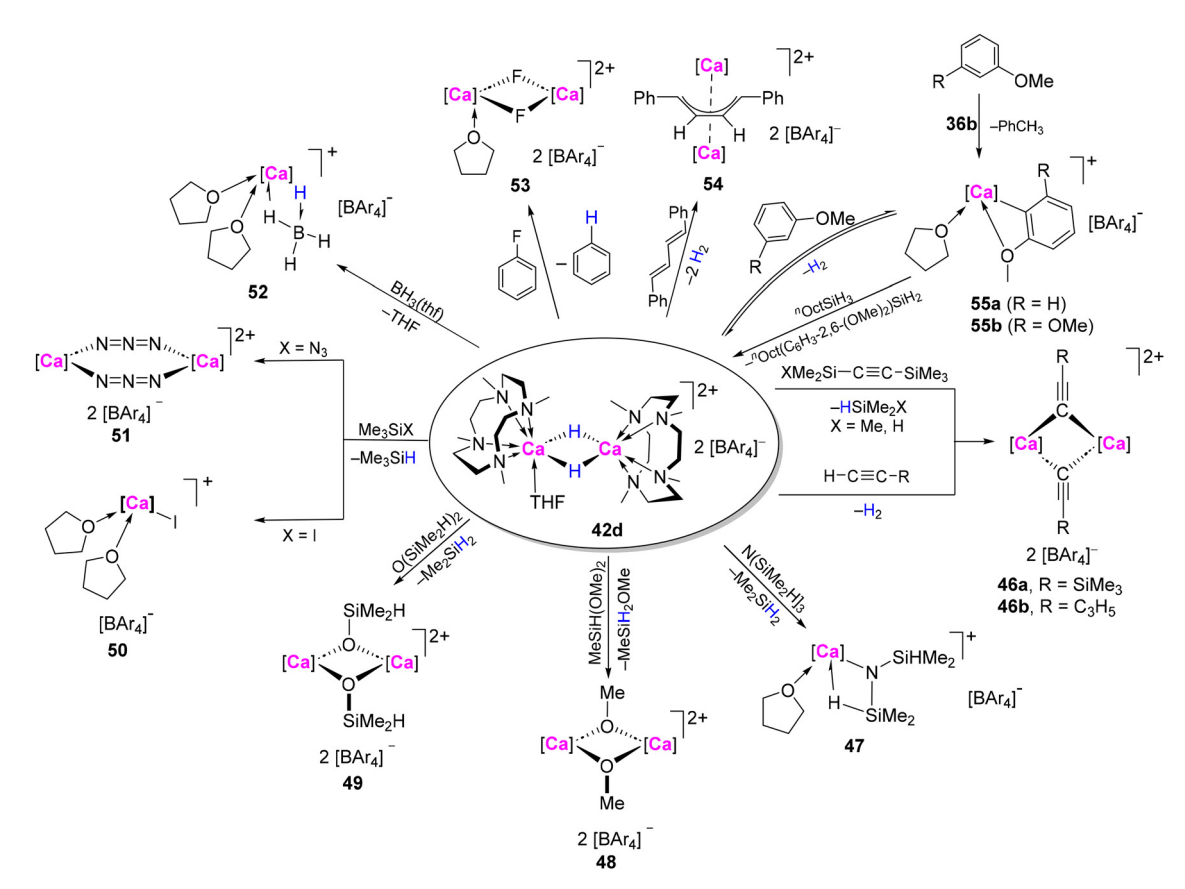
Insertion of unsaturated C-X multiple bonds. The nucleophilic hydrides of 42d readily insert CO2, forming the dimeric formate complex [(Me₄TACD)₂Ca₂(μ-OCHO)₂(thf)₂][B(C₆H₃-3,5- Me_2 ₄₂ (43, Scheme 15), ⁶⁵ and react with CO to yield the *cis*ethenediolate complex $[(Me_4TACD)_2Ca_2(OC(H)C(H)O)_2][B$ $(C_6H_3-3,5-Me_2)_4$ (44, Scheme 15). Monomerization of 42d was calculated to be only slightly endothermic; DFT calculations suggest that CO insertion occurs at the monomeric hydride $[(Me_4TACD)Ca(H)(thf)_x]^+$, providing a formyl intermediate that subsequently dimerizes into 44 (Scheme 15).65 The relative ease by which 42d can monomerize in THF solution carries important mechanistic implications in hydrofunctionalisation catalysis. Dimeric β-diketiminato magnesium and calcium

hydrides $[(BDI^{dipp})M(\mu-H)(thf)_n]_2$ (M = Mg, n = 0; M = Ca, n = 1) also react with CO to form cis-enediolates. 66-68 In these cases, however, the dimer is proposed to remain intact throughout the reaction, with a calculated mechanism involving initial two-fold hydride insertion to give an oxomethylene intermediate, followed by insertion of a second CO molecule and subsequent 1,2-hydride shift.

Ethylene readily inserts into the Ca-H bonds of 42d, forming the unstable ethyl-calcium complex [(Me4TACD)CaEt $(thf)_x^{\dagger}$ (45), observed via ¹H NMR spectroscopy. This species decomposes rapidly ($t_{1/2}$ = 10 min) into an intractable mixture.⁵⁴ Similar to [(BDI^{dipp})Ca(μ-H)]₂ and [(BDI^{dipep})Sr(μ-H)]₂ (BDI^{dipep} = HC{C(CH₃)N(C₆H₃-2,6-(C(H)Et₂)₂)}₂), 3,69 45 also reacts further with ethylene to generate labile calcium n-alkyl species. The nuclearity of 45 remains unclear; given the low energy barrier to hydride monomerization, which is proposed to occur during hydrogenation and hydrosilylation catalysis, 49,53,65,70 and the isolation of a related mononuclear seven-coordinate calcium ethyl cation [(Me5PACP)CaEt(thf)][B $(C_6H_3-3,5-Me_2)_4$, it is plausible that Me₄TACD-supported calcium n-alkyl complexes also exist as monomers in THF solution.

Nucleophilic and Brønsted-basic reactivity. The nucleophilic hydride of 42d reacts with alkynyl silanes Me₃SiC≡CSiMe₃ and HMe₂SiC≡CSiMe₃ via nucleophilic substitution, forming alkynyl calcium complex [(Me₄TACD)₂Ca₂(μ- $C \equiv CSiMe_3)_2 [B(C_6H_3-3,5-Me_2)_4]_2$ (46a) after elimination of Me₃SiH or Me₂SiH₂, respectively (Scheme 16).⁶⁵ Similarly, reaction with N(SiMe₂H)₃, MeSiH(OMe)₂, or O(SiMe₂H)₂ resulted

Scheme 15 Reactivity of compound 42d towards small molecules, and molecular structure of cis-enediolate 44. Ar = $C_6H_{3-}3,5-Me_2$.



Scheme 16 Reactivity of calcium hydride 42d. [Ca] = $[(Me_4TACD)Ca]^{2+}$; Ar = C_6H_3 -3,5-Me₂.

Dalton Transactions Perspective

nucleophilic substitution to form [(Me₄TACD)Ca $(N(SiHMe_2)_2)[B(C_6H_3-3,5-Me_2)_4]$ (47),[(Me₄TACD)₂Ca₂(µ- OMe_{2} [B(C₆H₃-3,5-Me₂)₄]₂ (48), or [(Me₄TACD)Ca(OSiMe₂H)][B $(C_6H_3-3,5-Me_2)_4$ (49) with elimination of Me_2SiH_2 or MeSiH₂OMe. 54,65 Whereas 48 crystallises as a dimer with bridging methoxide ligands, 47 is monomeric with an anagostic interaction between calcium and one of the Si-H bonds. Similarly, reactions with Me₃SiI and Me₃SiN₃ provide monomeric iodide, and dimeric azide complexes, [(Me4TACD)CaI $(thf)_2 \|B(C_6H_3-3,5-Me_2)_4\|$ (50) and $[(Me_4TACD)_2Ca_2(\mu-N_3)_2] \|B\|$ $(C_6H_3-3,5-Me_2)_4$ ₂ (51) after eliminating Me₃SiH.⁶⁵ Hydridic reactivity of 42d is also observed in the reaction with BH3. THF leading to tetrahydridoborate complex [(Me4TACD)Ca(BH4) $(thf)_2$ [B(C₆H₃-3,5-Me₂)₄] (52).⁶⁵ The strong nucleophilicity of 42d enables nucleophilic aromatic substitution with fluorobenzene, cleaving the C_{sp2}-F bond to form the dimeric fluoride complex $[(Me_4TACD)_2Ca_2(\mu-F)_2(thf)][B(C_6H_3-3,5-Me_2)_4]_2$ (53) with benzene elimination.⁶⁵ Structurally, 53 resembles the parent hydride, with two fluoride ligands bridging six- and seven-coordinate calcium centres. As a strong Brønsted base, **42d** deprotonates RC \equiv CH (R = SiMe₃, C₃H₅) to yield dimeric acetylides, 46a and $[(Me_4TACD)_2Ca_2(\mu-C \equiv CC_3H_5)_2][B(C_6H_3-3,5-$ Me₂)₄]₂ (46b), and reacts with trans, trans-1, 4-diphenylbuta-

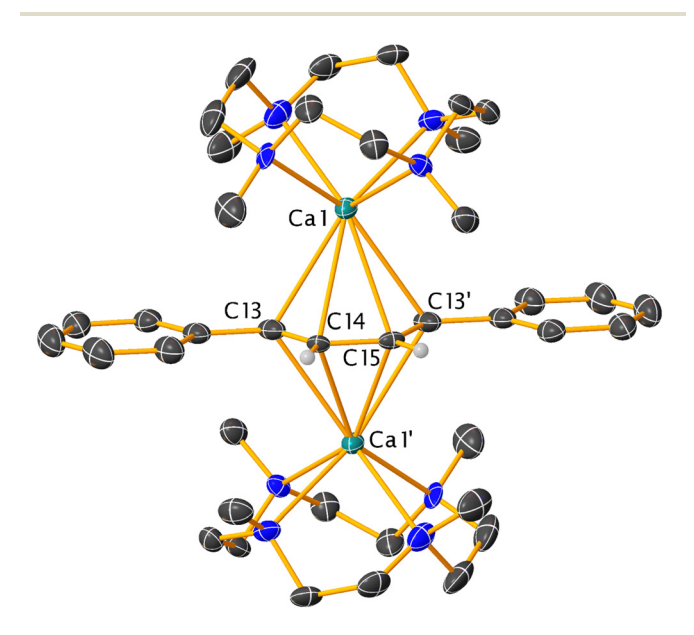


Fig. 5 Molecular structure of the dicationic part of the butadienyl calcium complex 54.65

diene to provide the dinuclear butadienyl complex $[(Me_4TACD)_2Ca_2(\mu_2-\eta^4-1,4-Ph_2C_4H_2)][B(C_6H_3-3,5-Me_2)_4]_2$ (Fig. 5). Anisole and 1,3-dimethoxybenzene are deprotonated, forming aryl-calcium complexes [(Me₄TACD)Ca(κ²-O,C-C₆H₄-6-OMe)(thf)][$B(C_6H_3-3,5-Me_2)_4$] (55a) and [(Me₄TACD)Ca(κ^2 -O, $C-C_6H_4-2,6-(OMe)_2$ (thf)][B($C_6H_3-3,5-Me_2$)₄] (55b).⁴² Compound 55**b** undergoes σ-bond metathesis with n OctSiH₃ to regenerate **42d** under elimination of ${}^{n}Oct(C_{6}H_{3}-2,6-(OMe)_{2})SiH_{2}$.

4.2.4. Catalysis mediated by molecular calcium hydride complexes. The dinuclear trihydride-silanide salt 41a reacts with 1,1-diphenylethylene by silicon-centred nucleophilic addition to give {(triphenylsilyl)methyl}diphenylmethanide salt **41e** (Scheme 17).⁵⁰

The calcium complex 41e catalyses the hydrogenation of 1,1'-diphenylethylene at 60 °C within 24 h under 1 bar H₂, likely via Ca-H insertion and subsequent σ -bond metathesis (Scheme 18a). The borate-salt 41c catalysed the same reaction in 12 h at 25 °C, whilst the dicationic dihydride 42b is more active, achieving 98% conversion in 6 h under ambient conditions. 49 42b also catalyses the hydrogenation of styrene (10 h, 25 °C), 1,2-diphenylethylene (24 h, 60 °C), triphenyl-(16 h, 60 °C) and (trimethyl)vinylsilane (36 h, 60 °C). Catalytic activity was not restricted to activated alkenes; 1-hexene, 1-octene, 3-vinylcyclohexene, 1,5-hexadiene, and 1,9-decadiene were also hydrogenated (Scheme 18b). Dihydride 42b displayed higher activity than trihydride 41c. No hydrogenation of internal double bonds (3-vinylcyclohexene, cyclohexene) was observed. For 1-hexene, 1-octene, 1,5-hexadiene, and 1,9-decadiene, 5% 2-alkene was observed in the product mixture; for 1,5-hexadiene, 4% of the cyclisation product methylcyclopentane was also formed.

The activity of compounds 41c.e., and especially 42b in alkene hydrogenation compares well with other alkaline-earth catalysts. Bulky cyclopentadienyl-derivatives $[(\eta^5-C_5R_5)_2M_2(\mu H_{2}(L)$ (M = Ca, Sr, Ba; R = $C_{6}H_{3}$ -3,5- 1 Pr; L = THF or DABCO) also catalyse alkene hydrogenation, including unactivated n-alkenes at 30 °C under 6 bar H₂, with activity increasing with metal size.⁷¹ By comparison, a magnesium PNP pincer $[\{C_5H_3N(C(H)P^tBu_2)(CH_2P^tBu_2)\}_2Mg_2Et_2(\mu-1,4-1)]$ dioxane)] was reported to catalyse the hydrogenation of alkenes including unactivated 1-dodecene, 1-octene, 3-(orthomethoxy)phenyl-prop-1-ene, 4-phenyl-but-1-ene, and 3-(trimethylsilyl)-prop-1-ene, but requires harsh conditions (120 °C, 5 bar). 72 A related calcium-based system was limited to activated substrates like 1,1'-diphenylethene and styrene.⁷³ The β-diketiminato derivative $[(BDI^{dipp})Ca(\mu-H)(thf)]_2$ catalyses the

Scheme 17 Silanide-centred reactivity of 41a towards 1,1'-diphenylethene.

Scheme 18 Hydrogenation of (a) activated, (b) unactivated alkenes catalysed by calcium hydrides 41c,e, and 42b.

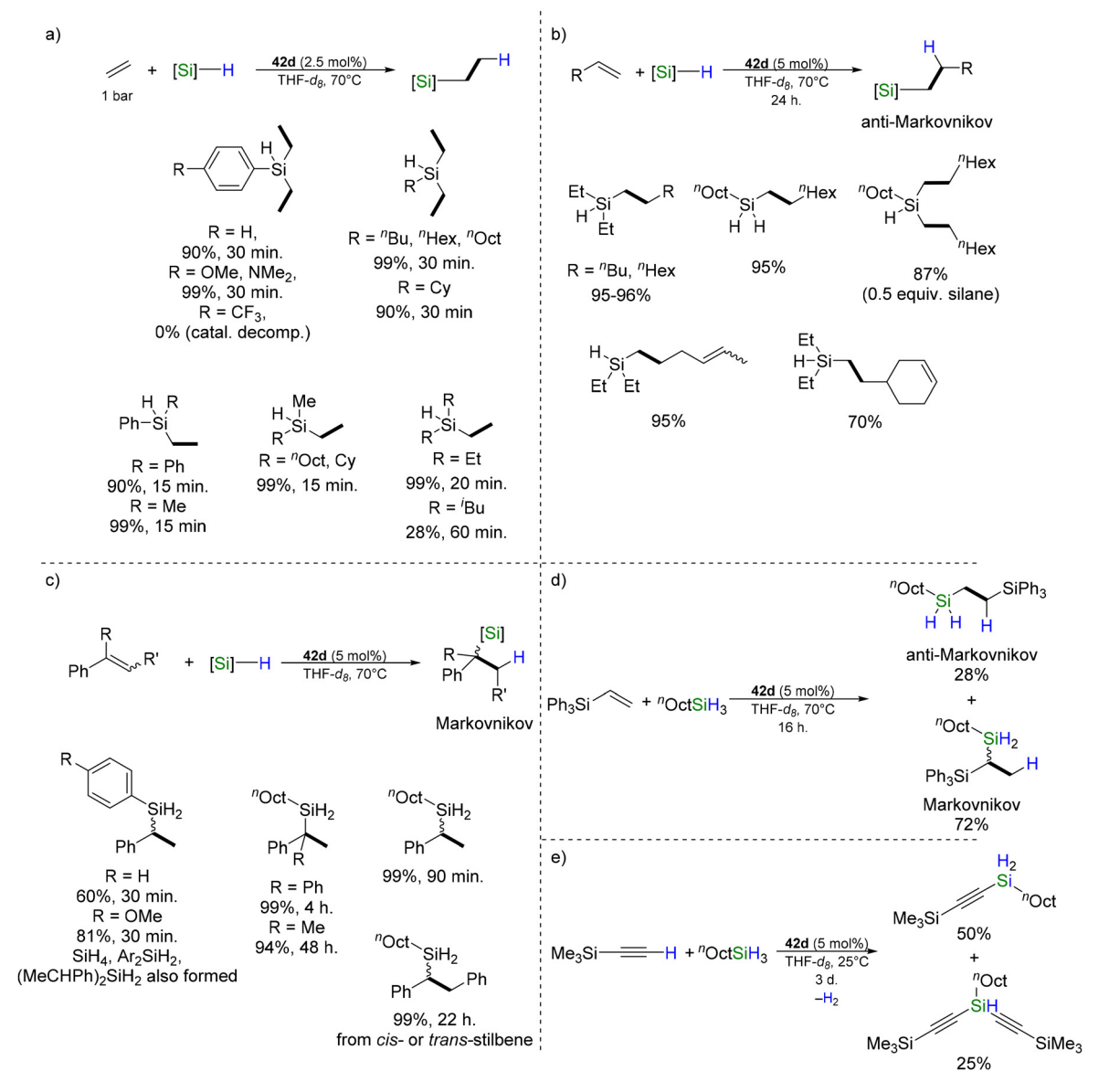
hydrogenation of 1,1'-DPE and styrene derivatives at 60 °C under 20 bar H₂ pressure.⁷⁴ In contrast, the unsolvated analogue $\lceil (BDI^{dipp})Ca(\mu-H) \rceil_2$ catalyses the hydrogenation of unactivated n-alkenes at ambient conditions, 75 although catalysis was limited to room temperature with slow conversion (21 d), due to competitive nucleophilic alkylation of benzene at elevated temperature.^{3,75} The Me₄TACD-based systems are thermally robust, permitting mildly elevated temperatures and appreciable rates. High activity compared to [(BDI^{dipp})Ca(μ-H) (thf)]₂ ⁷⁴ was attributed to a high degree of Lewis acidity and facile monomerization due to cationic charge. Notably, heavier alkaline-earth amides $[Ae(NRR')_2]_n$ (R = SiMe₃, SiⁱPr₃; R' = SiMe₃, Si¹Pr₃, C₆H₃-2,6-¹Pr₂) act as pre-catalysts for the efficient hydrogenation and transfer hydrogenation of challenging unactivated n-alkenes, as well as internal secondary alkenes and aromatic rings under relatively mild conditions (up to 120 °C, 1-6 bar H₂). 58,59,76,77 Here, multinuclear (amido)alkaline-earth hydride clusters are proposed as active species, with bulkier amides leading to lower nuclearity and higher activity.

Hydride 42d also catalysed alkene hydrosilylation.⁵⁴ Ethylene was hydrosilylated by various aromatic and aliphatic hydrosilanes at 70 °C in under 60 min (Scheme 19a). Primary and secondary hydrosilanes yielded di- and monoethylated silanes. Longer-chain aliphatic n-alkenes were hydrosilylated more slowly (24 h, 70 °C, conversion 70-96%) with anti-Markovnikov regioselectivity (Scheme 19b). Markovnikov products were observed for aryl-substituted olefins (Scheme 19c), as the result of a π -interaction of the phenyl group with the Lewis-acidic Ca centre. A mixture of Markovnikov and anti-Markovnikov products was obtained for the hydrosilylation of triphenyl(vinyl)silane with *n*-octylsilane. Internal double bonds were not hydrosilylated. Arylsilanes undergo scrambling reactions promoted by the electrophilic calcium hydride (Scheme 14), providing SiH₄ and Ph₂SiH₂ in the case of phenylsilane, and alkoxy and siloxy calcium derivatives (e.g., 48, 49, Scheme 16)54,65 from alkoxy- and siloxy-substituted hydrosilanes, thus making aliphatic hydrosilanes preferable. Attempted hydrosilylation of terminal alkyne HC≡CSiMe₃ with "OctSiH₃ using 5 mol% **42d** instead provided dehydrocoupling products $(Me_3SiC = C)(^nOct)SiH_2$ and $(Me_3SiC = C)_2(^nOct)SiH$ in a 2:1 ratio (Scheme 19e). 42

Monomerization of $[(Me_4TACD)_2Ca_2(\mu-H)_2(thf)_x]^{2+}$ to give a reactive terminal hydride species [(Me₄TACD)Ca(H)(thf)_v]⁺ was suggested to precede alkene insertion and catalytic turnover (Scheme 20). While monomeric hydride or alkyl-derivatives were not isolated for Me, TACD, a mononuclear terminal ethyl complex [(Me₅PACP)CaEt(thf)][B(C₆H₃-3,5-Me₂)₄], was crystallised for the larger 15-membered macrocycle, Me₅PACP.⁵³ Further, kinetic studies on the hydrosilvlation of 1-octene by n-octylsilane showed a 1/2-order dependence on dimeric hydride pre-catalyst for both 42d and [(Me₅PACP)₂Ca₂(μ-H)₂][B(C₆H₄-4-ⁿBu)₄]₂, implying a monomeric active species in both cases.⁵³ Despite increased steric and coordinative demand, the Me₅PACP derivative was more active than 42d, likely due to easier access to mononuclear species for the larger ligand. Catalysis is first-order in 1-octene and pseudo-zeroth order in *n*-octylsilane, suggesting rate-limiting alkene insertion and rapid σ-bond metathesis of the *n*-alkyl intermediate with hydrosilane.

When compared with the similarly dimeric pre-catalyst $[(BDI^{dipp})Ca(\mu-H)]_2$ (Scheme 20), dimeric alkyl-hydride species $[(BDI^{dipp})_2Ca_2(\mu-H)(\mu-R)]$ (R=n-alkyl) were observed by *in situ* NMR spectroscopy as a resting-state in the catalytic run, indicating a persistent dimeric active species, slow insertion of alkene into the second μ -H, and rate-limiting σ -bond metathesis with H_2 .⁷⁵ Dimeric dialkyl insertion products $[(BDI^{dipp}) Ca(\mu-R)]_2$ could be isolated in the absence of H_2 .^{3,75,78} Conversely, the hydride resonance in the ¹H NMR spectrum of **42b**-mediated n-alkene hydrogenation remained unchanged in catalysis, and attempts to isolate insertion products of 1-hexene or 3-vinylcyclohexane failed, suggesting reversible and rate-limiting alkene insertion/β-hydride elimination and rapid σ -bond metathesis with H_2 .^{49,53}

The hydrosilylation of unactivated n-alkenes using phenylsilane has also been reported for the dimeric magnesium precatalyst $[(BDI^{dipp})Mg(\mu-H)]_2$. Near-quantitative conversion was achieved in over 4 d at 60 °C, with bulkier or aryl alkenes like styrene showing reduced activity. Similar to the calcium analogue, n-alkene insertion was calculated to occur at the



Scheme 19 Hydrosilylation of olefins catalysed by 42b: (a) hydrosilylation of ethylene; (b) anti-Markovnikov selective hydrosilylation of aliphatic 1-alkenes; (c) Markovnikov selective hydrosilylation of styrene derivatives; (d) hydrosilylation of triphenyl(vinyl)silane with mixed selectivity; (e) dehydrocoupling of trimethylsilylacetylene and n-octyl silane.

intact dimeric µ-hydride complex rather than through mononuclear species, although ready dissociation of the resultant mixed hydride-alkyl species $[(BDI^{dipp})_2Mg_2(\mu\text{-}H)(\mu\text{-}R)]$ implimixed cates mononuclear on-cycle intermediates during catalysis (Scheme 20). The faster reaction rates observed for 42b compared to [(BDI^{dipp})Mg(μ-H)]₂ are likely due to calcium's lower electronegativity, stronger polarization, and lower steric hindrance at the metal centre, facilitating more efficient alkene activation and hydrosilylation. The cationic charge of the active species may also play a role in promoting the coordination and polarisation of alkene and silane during catalysis.

The mechanism of the hydrogenation of 1-alkenes mediated by [(Me₄TACD)₂Ca₂(μ-H)₂]²⁺ as pre-catalyst was studied computationally. 70 A mechanism involving an intact μ-

H bridged dimer was computed to be more energetically favourable for H2 isotope exchange than with a mononuclear terminal hydride. Anti-Markovnikov addition of aliphatic 1-alkenes was competitive for either hydride-bridged dimer or mononuclear terminal hydride [(Me₄TACD)Ca(H)(thf)]⁺, whilst Markovnikov addition of styrene was observed for the mononuclear hydride, influenced by Ca^{\dagger} -Ph cation- π interactions, which directed regioselectivity.

In summary, it appears that the ability for chelating polydentate aza-macrocycles to infer relatively high stability towards highly Lewis acidic mononuclear calcium cations may play an important role in the comparatively high activity of calcium hydride complexes 42b,d as pre-catalysts for hydrogenation and hydrosilylation of unactivated alkenes.

Dicationic dimer, aza-macrocycle Neutral dimer, β -diketiminate

Scheme 20 Contrast in proposed mechanisms for olefin hydrogenation and hydrosilylation mediated by Me₄TACD/Me₅PACP-calcium and BDI^{dipp}-calcium/magnesium catalysts.

4.3. Strontium

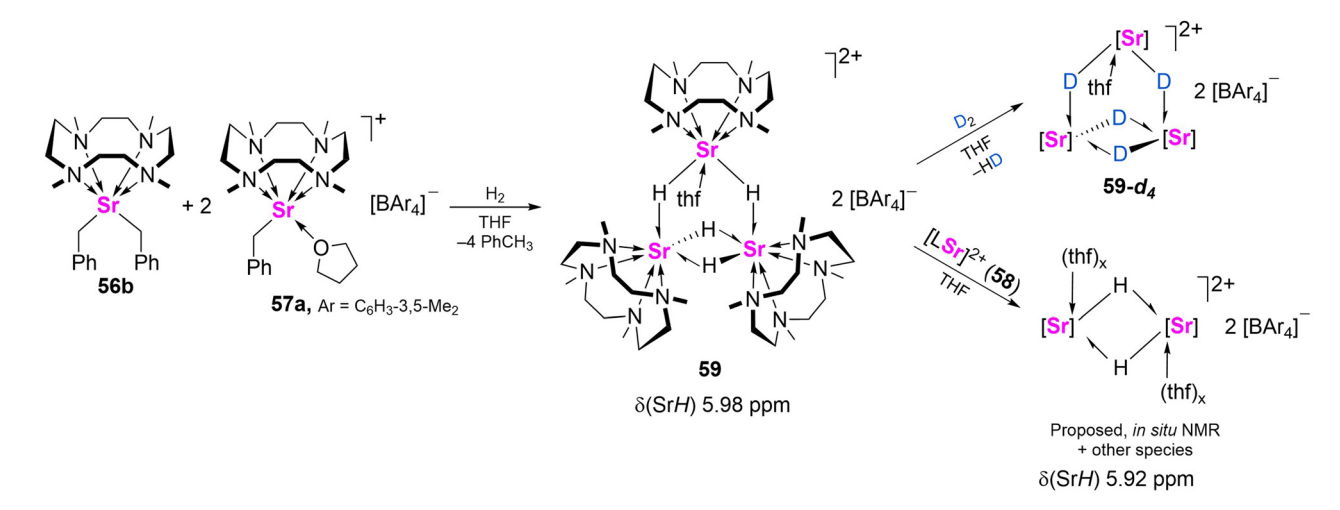
4.3.1. Organostrontium complexes. The dibenzyl strontium complex, [(Me₄TACD)Sr(CH₂Ph)₂(thf)] (56a) was synthesised by combining Me₄TACD and [Sr(CH₂Ph)₂(thf)] in (Scheme 21).80 The crystal structure of 56a consists of a sevencoordinate metal centre with two n¹-coordinated benzyl ligands and one coordinated THF. Coordinated THF was found to be labile, giving the six-coordinate dibenzyl complex [(Me₄TACD)Sr(CH₂Ph)₂] (56b) under vacuum. Protonation of 56b with the Brønsted acid [NEt₃H][BAr₄] (1 or 2 equiv.) produced the respective benzyl strontium cation [(Me₄TACD)Sr $(CH_2Ph)(thf)[BAr_4]$ (57a, Ar = C₆H₃-3,5-Me₂; 57b, Ar = C₆H₄-4-"Bu) and bis-borate dication [(Me₄TACD)Sr(thf)₂][B(C₆H₃-3,5- Me_2 ₄₂ (58). The coordination sphere of the { Me_4 TACD)Sr} unit appears rather flexible, adopting coordination numbers of either six or seven. Further, η¹-benzyl cation 57a loses THF under vacuum to provide the slipped η^6 -benzyl complex $[(Me_4TACD)Sr(CH_2Ph)][B(C_6H_3-3,5-Me_2)_4]$ (57c), which could also be synthesised by protonolysis of 56b with [NEt₃H][B $(C_6H_3-3,5-Me_2)_4$ in THP. The crystal structure of 57c closely resembles the THF-free η^6 -benzyl calcium complex 36d (Scheme 8).⁴² Unlike 36b, 57a did not deprotonate the borate anion to form a zwitterionic complex similar to 38.

4.3.2. Strontium hydride complexes. Me₄TACD appears less effective at stabilizing low-nuclearity strontium hydride complexes compared to calcium due to the larger ionic radius, lower charge density, and more ionic Sr–H bonds. Indeed, structurally characterised molecular strontium hydride complexes are less common compared to the lighter group 2 elements. Whilst simple amides and chelating amines can stabilise strontium hydride clusters, ^{56,57} extremely bulky ligands are generally necessary to isolate di- and trinuclear complexes. ^{69,71,81,82}

Whilst hydrogenolysis or silanolysis of **36** provides access to dimeric calcium dihydride, hydrogenolysis of **57a** in THF leads to a complex mixture. ⁸⁰ A single species repeatedly crystallised from these solutions, and was structurally characterised as the trinuclear cluster dication, $[(Me_4TACD)_3Sr_3(\mu-H)_4(thf)][B(C_6H_3-3,5-Me_2)_4]_2$ (**59**), which can be rationally synthesised by hydrogenating a 2:1 mixture of **57a** and **56b** (Scheme 22).

The trinuclear dication of 59 (Fig. 6) consists of three sevencoordinate strontium centres and can be described as an **Dalton Transactions**

Scheme 21 Synthesis of dibenzyl strontium complexes 56a,b, cationic benzyl complexes 57a-c, and strontium bis(borate) salt 58. Molecular structure of the cationic part of 57c, with benzylic hydrogen atoms shown.



Scheme 22 Synthesis of trinuclear strontium hydride 59, isotopic exchange with D₂, and proposed formation of dimeric [L₂Sr₂H₂]²⁺ species in solution.

adduct of $[(Me_4TACD)SrH_2(thf)]$, and $[(Me_4TACD)_2Sr_2(\mu-H)_2]^{2+}$ units, or of two [(Me₄TACD)SrH₂] units and a [(Me₄TACD)Sr (thf)]²⁺ dication. Sr1 bridges Sr2 and Sr3 via a hydride ligand and coordinates to a THF ligand, while Sr2 and Sr3 share two bridging hydrides. The ¹H NMR spectrum reveals two distinct {(Me₄TACD)Sr} environments, with a single hydride resonance

at δ 5.98 ppm, indicating rapid hydride exchange between the distinct strontium centres even at −60 °C. Complex 59 rapidly exchanges with D₂, providing the fully deuterated isotopologue after 30 min at room temperature (Scheme 22). Combining 59 and 58 resulted in an additional hydride resonance at δ 5.92 ppm in the ¹H NMR spectrum, which was tentatively

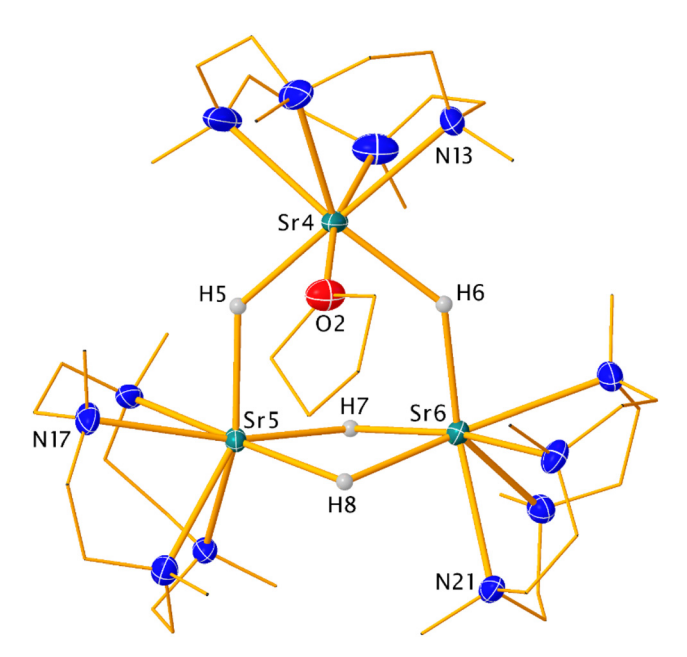


Fig. 6 Molecular structure of the cationic part of trinuclear strontium hydride 59.80

assigned to the elusive $[(Me_4TACD)_2Sr_2(\mu+H)_2(thf)_x]^{2+}$, although attempts to isolate it remained unsuccessful. Me_4TACD lacks sufficient steric and coordinative demand to prevent redistribution. A stable $[Sr_2H_2]^{2+}$ dication, $[(Me_5PACP)_2Sr_2(\mu-H)_2][B(C_6H_3-3,5-Me_2)_4]_2$, was isolated using the larger 15-membered macrocycle Me_5PACP .

Hydrogenation of an equimolar THF solution of **57a** and **36b** provided the heterobimetallic hydride complex $[(Me_4TACD)_2CaSr(\mu-H)_2(thf)][B(C_6H_3-3,5-Me_2)_4]_2$ (**60**; Scheme 23), which is isostructural to **42d**. ⁵⁴ The crystal structure of **60** revealed a $Ca(\mu-H)_2Sr$ core, where the calcium is sixcoordinate and the strontium is seven-coordinate with an

additional THF ligand. The ¹H NMR analysis of **60** in THF-d₈ showed a major hydride resonance at δ 5.10 ppm, intermediate between homometallic Sr hydride 59 (δ 5.98 ppm) and Ca hydrides 41 (δ 4.72 ppm) and 42 (δ 4.45 ppm).⁸⁰ Notably, resonances corresponding to calcium hydride dimers 41 and 42, and several broad resonances between δ 5.98 and 5.92 ppm for strontium hydrides, were also observed in the spectrum. ¹H-¹H EXSY experiments confirmed rapid exchange between these species, suggesting facile dissociation and recombination of 60 in solution. Thermodynamic studies indicated that Ca-H bonds are more favourable than Sr-H bonds, as excess [(L)Ca]²⁺ shifted the equilibrium toward calcium hydrides. Mixing calcium bis-borate 37b with calcium-strontium hydride 60 resulted in the selective formation of calcium hydride dimer 41 and strontium bis-borate 58. Conversely, combining 58 and 60 resulted in the persistence of 60 as the major species, with minor quantities of 41 and 42 and traces of postulated $[(Me_4TACD)_2Sr_2(\mu-H)_2(thf)_x][B(C_6H_3-3,5-Me_2)_4]_2$. Complexes 59 and 60 catalyse n-alkene hydrogenation, 80 but quantitative activity comparison with homometallic calcium hydride dimers 41 and 42 is not appropriate due to the aforementioned hydride lability and poorly-defined solution-state speciation.

4.3.3. Strontium hydridosilicate and silanide complexes. Me₄TACD-ligated organocalcium complexes can be converted to molecular hydrides via hydrogenation or hydridosilanes. However, reacting 57 with RSiH₃ (R = Ph, n Oct) led to a different outcome compared to hydrogenolysis. When PhSiH₃ was employed, Ph(PhCH₂)SiH₂, Ph₂(PhCH₂)SiH, and SiH₄ were observed in the *in situ* 1 H NMR spectrum, indicating σ-bond metathesis with the benzyl precursor and subsequent organosilane scrambling. The dinuclear hexahydridosilicate complex [(Me₄TACD)₂Sr₂(μ-κ³:κ³-SiH₆)(thf)₄][BAr₄]₂ (**61a**, Ar = C₆H₃-3,5-Me₂; **61b**, Ar = C₆H₄-4- n Bu) was isolated in high yields (91%, **a**; 69%, **b**) (Scheme 24). Compounds **61** are thermola-

Scheme 23 Synthesis of Sr/Ca hydride 60 and hydride exchange reactions with 37b and 58 in solution. 1 H NMR chemical shifts are shown for diagnostic hydride resonances. Ar = C_6H_3 -3,5-Me₂.

Dalton Transactions Perspective

Scheme 24 Synthesis of strontium hydridosilicate complexes 61a,b and 64, and silanide complexes 62a,b and 63.

bile, decomposing at room temperature with dihydrogen release (also detected by ¹H NMR spectroscopy), forming the mononuclear parent silanide complex, [(Me4TACD)Sr(SiH3) $(thf)_2$ [BAr₄] (62a, Ar = C₆H₃-3,5-Me₂; 62b, Ar = C₆H₄-4-ⁿBu). 63 The reaction can be formally considered as the net-reductive elimination of dihydrogen from the hypervalent Si(IV) centre, and dissociation of the putative strontium hydride cation $[(Me_4TACD)SrH(thf)_x]^+$. A 2:1 mixture of 57a and 57b with excess phenylsilane at room temperature produced the trinuclear hydride-silanide cluster, [(Me₄TACD)₃Sr₃(μ-H)₃(μ₃-SiH₃)₂][B $(C_6H_3-3,5-Me_2)_4$ (63). The observed evolution of H_2 in this reaction also suggests the dehydrogenation of a hypervalent silicate species.

Similarly, the synthesis and isolation of a carbozolido barium silanide complex via metathesis of a hexamethyldisilazide precursor with PhSiH3 has been reported; the {SiH₃} moiety was found to act either as nucleophilic silanide, or as a hydride surrogate.83 Heavy alkaline-earth elements facilitate hydrido(aryl)silanes redistribution, but using ⁿOctSiH₃ as hydride source suppresses such redistribution reactions, yielding the trinuclear hydride-hydridosilicate cluster, $[(Me_4TACD)_3Sr_3(\mu-H)_3(\mu_3-SiH_5(^nOct))][B(C_6H_3-3,5-Me_2)_4]$ (64) with the *n*-alkyl group intact. Compound 64 was rationally synthesised in 65% yield by reacting a 2:1 mixture of 56b and

57a with a ten-fold excess of "OctSiH₃ (Scheme 24). These complexes likely result from two-fold nucleophilic addition of highly reactive [(Me₄TACD)SrH]⁺ units to either SiH₄ (derived from [(Me₄TACD)SrH]⁺ mediated organosilane scrambling), or ⁿOctSiH₃. This interpretation corroborates with the broadened and exchanging hydride resonances observed for calcium hydride 42d and PhSiH3 mixture, where Ph2SiH2 and SiH4 are also observed, implicating hydridosilicate species.⁵⁴

Similar hydridosilicate complexes were not isolated for the analogous reaction of either 36, 39, 42,54 or [(Me₅PACP)Sr $(CH_2Ph)(thf)[BAr_4] (Ar = C_6H_3-3,5-Me_2 \text{ or } C_6H_4-4^nBu)^{52} \text{ with}$ RSiH₃, suggesting that the kinetic stability of 61 depends on the high nucleophilic character of the Sr-H bonds, and the moderate size of the Me₄TACD ligand relative to the ionic radius of Sr²⁺. Previously, a dinuclear ruthenium hexahydridosilicate complex $[\{(PhB(CH_2PPh_2)_3)Ru\}_2\{\mu-\eta^4,\eta^4-SiH_6\}]$ was reported.⁸⁴ In this case, the {SiH₆} unit binds to the ruthenium centres via covalent 3-centre-2-electron bonding interactions. By contrast, the interaction between Sr and $\{SiH_6\}$ in **61** is predominantly electrostatic, as indicated by NMR and vibrational spectroscopy, as well as DFT calculations. Recently, a comparable calcium-potassium hexahydridosilicate $[(NON)_2Ca_2K_2(\mu_4-\kappa^3:\kappa^3:\kappa^2:\kappa^2-SiH_6)(thf)_2]$ (NON = 4,5-bis(2,6diisopropylanilido)-2,7-di-tert-butyl-9,9-dimethyl-xanthene) was

Perspective **Dalton Transactions**

reported, and similarly reacts as a masked metal hydride elimination.⁶⁴ under SiH₄ Unlike 61, $[(NON)_2Ca_2(\mu_4-\kappa^3:\kappa^3:\kappa^2:\kappa^2-SiH_6)(thf)_2]$ is stable in benzene at room temperature, probably due to a more robust binding cavity offered by the tetranuclear Ca2K2 assembly compared to the labile dinuclear structure of 61. A strontium-potassium pentahydrido(aryl)silicate complex $[(NON)_2Sr_2K_2(\mu_4-\kappa^3:\kappa^3:\kappa^2:\kappa^2-\kappa^2]$ PhSiH₅)(thf)₂] reminiscent of **64** was also reported.⁶⁴

Single crystal X-ray diffraction revealed the cationic part of 61 to formally contain an [SiH₆]²⁻ dianion sandwiched in a $\mu - \kappa^3 : \kappa^3$ -fashion between two $[(Me_4TACD)Sr(thf)_2]^{2+}$ dications (Fig. 7). The dinuclear core exhibits flexibility around the Sr-Sr axis. In the solid-state, 61a contains a non-centrosymmetric dication with a gauche arrangement of the neutral ligands on each Sr, whilst 61b is crystallographically centrosymmetric, with an anti-periplanar arrangement.

Compound 61 was characterised by NMR spectroscopy at low temperatures due to its instability in THF above 0 °C. In the ¹H NMR spectrum, the hydrides appeared as a singlet at δ 5.39 ppm, sharpening when cooled to -40 °C. Direct ²⁹Si NMR measurement of 61 was unsuccessful, but at -40 °C, a signal was observed by $^{29}\text{Si}^{-1}\text{H}$ HSQC and HMBC experiments at δ_{Si} -172.6 ppm, appearing as a doublet with a coupling constant $J(^{29}Si^{-1}H) = 118$ Hz. These spectroscopic features indicate largely ionic Sr-H bonding interactions and thus a relatively unperturbed [SiH₆]²⁻ dianion compared to [{(PhB(CH₂PPh₂)₃) $Ru_{2}\{\mu-\eta^{4},\eta^{4}-SiH_{6}\}\]$, whose more covalent Ru-H bonding results in smaller 29Si-1H coupling constant, upfield shifted ²⁹Si resonance in the NMR spectrum, and longer Si-H distances.84 Similarly, $[(NON)_2Ca_2(\mu_4-\kappa^3:\kappa^3:\kappa^2:\kappa^2-SiH_6)(thf)_2]$ exhibited hydride resonances at δ 5.38 ppm, and a ²⁹Si signal at δ –261.2 ppm.⁶⁴ A Si-H stretching absorption was observed in the ATR-IR spectrum of **61a** at $\nu = 1717 \text{ cm}^{-1}$, similar to previously reported values for K2SiH6 and [{(PhB(CH2PPh2)3) $Ru_{2}\{\mu-\eta^{4},\eta^{4}-SiH_{6}\}\]$. In contrast, the ATR-FTIR spectrum of $[(NON)_2Ca_2(\mu_4-\kappa^3:\kappa^3:\kappa^2:\kappa^2-SiH_6)(thf)_2]$ showed three bending

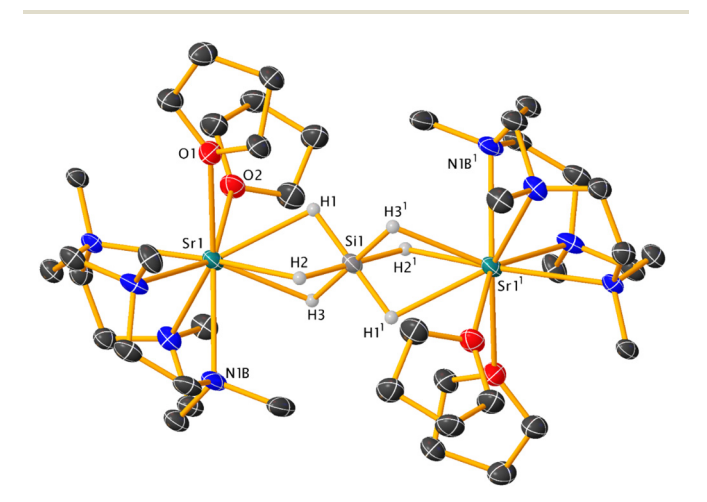


Fig. 7 The molecular structure of dication [61b]²⁺, with only siliconbound hydrogen atoms.54

modes at 1053, 1013, and 976 cm⁻¹, and three stretching modes at 1620, 1558, and 1503 cm⁻¹.64

The crystal structure of 64 features a triangular Sr₃ core with each metal bridged by a μ-H ligand, while an octahedral ["OctSiH₅] unit bridges all three metals via four equatorial hydrides and one terminal hydride (Fig. 8). ¹H NMR spectroscopy shows rapid hydride exchange at room temperature, giving a broad resonance at δ 5.66 ppm, which splits into a complex pattern of resonances at −80 °C. At −80 °C, a resonance at δ_{Si} 112.4 ppm was observed in a $^{29}Si^{-1}H$ HSQC experiment. The crystal structure of 63 contains a similar μ-H bridged triangular Sr₃ core to that in 64, with the trigonal bipyramidal cluster capped by two μ₃-SiH₃ ligands.

Compound 61 acts as a masked equivalent of the elusive dimeric strontium hydride $[(Me_4TACD)_2Sr_2(\mu-H)_2(thf)_x]^{2+}$; reacting with Brønsted acid [NEt3H][B(C6H3-3,5-Me2)4], CO2, or oxidant 1,3,5,7-cyclooctatetraene (COT), to eliminate SiH4 and yield strontium hydride-based products (Scheme 25). Specifically, $[NEt_3H][B(C_6H_3-3,5-Me_2)_4]$ yielded the bis(borate) salt 58, CO₂ provided the dimeric formate [(Me₄TACD)₂Sr₂(μ-OCHO)(thf)₂][$B(C_6H_3-3,5-Me_2)_4$]₂ (65), and COT was reduced under loss of H2 to form the dinuclear inverse sandwich compound $[(Me_4TACD)_2Sr_2(\mu-\eta^8:\eta^8-COT)][B(C_6H_3-3,5-Me_2)_4]_2$ (66).⁶³ Based on literature precedent for the formation of [(BDI^{dipp})₂Ca₂COT], 85 66 is most likely formed through an even-electron insertion-deprotonation sequence, rather than via two-fold single electron reduction of the conjugated tetraene. It is noteworthy that calcium hydride complex 42d is unreactive towards COT; formation of $[(Me_4TACD)_2Ca_2(\mu-\eta^8:\eta^8-\eta^8)]$ COT) $[B(C_6H_3-3,5-Me_2)_4]_2$ (67) was instead achieved by in situ reduction with caesium metal and salt metathesis of iodide complex 50.42

4.4. Barium

The molecular coordination chemistry of barium is far less studied than that of lighter group 2 elements, especially for organo- and hydridobarium complexes. The large size, extremely low electronegativity, and dominance of undirectional ionic bonding make isolating well-defined, low-nuclearity, and heteroleptic complexes a significant challenge.86

Neutral and cationic Me₄TACD barium benzyl complexes were prepared using a method similar to that of lighter homologues. Adding Me₄TACD to a THF-suspension of [Ba(CH₂Ph)₂] yields a yellow solution from which the neutral dibenzyl [(Me₄TACD)Ba(CH₂Ph)₂] complex (68)crystallised (Scheme 26).87 Comparing its crystal structure to related calcium (34) and strontium (56a) complexes highlights differences in coordination. Whereas 34 contains a six-coordinate calcium centre and two n¹-benzyl ligands, the larger Sr²⁺ cation accommodates an additional THF molecule, with both benzyl ligands remaining η¹-bound. Whilst the still-larger Ba²⁺ is expected to adopt a yet-higher coordination number via ligation of additional solvent molecules, 68 is THF-free, and the coordination sphere is satisfied by slipped η^2 and η^3 -bound benzyl ligands. This is consistent with the high lability of Ba-THF bonds and π -acidity of the softer metal cation.

Dalton Transactions Perspective

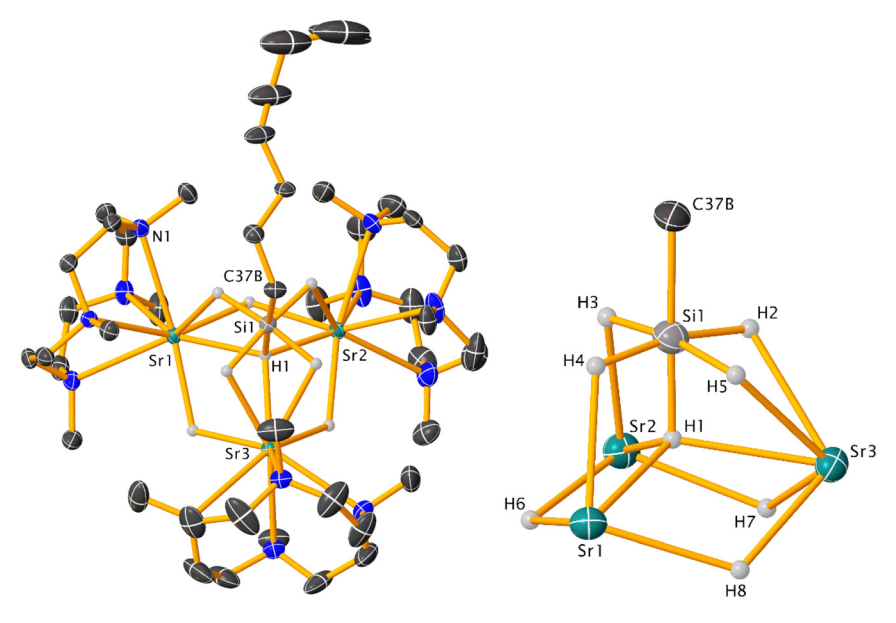


Fig. 8 Cationic part of the molecular structure of compound 64 with hydrogen atoms omitted except for hydride ligands (left); the $\{Sr_3H_3(RSiH_5)\}$ core of 64 without ligands and n-octyl chain (right).⁵⁴

Protonolysis of **68** with [NEt₃H][B(C₆H₃-3,5-Me₂)₄] provided the cationic benzyl complex [(Me₄TACD)Ba(CH₂Ph)(thf)_x][B(C₆H₃-3,5-Me₂)₄] (**69**), which was not crystallographically characterised, but shows downfield shifted CH_2 resonance in the ¹H NMR, suggesting increased benzyl hapticity.

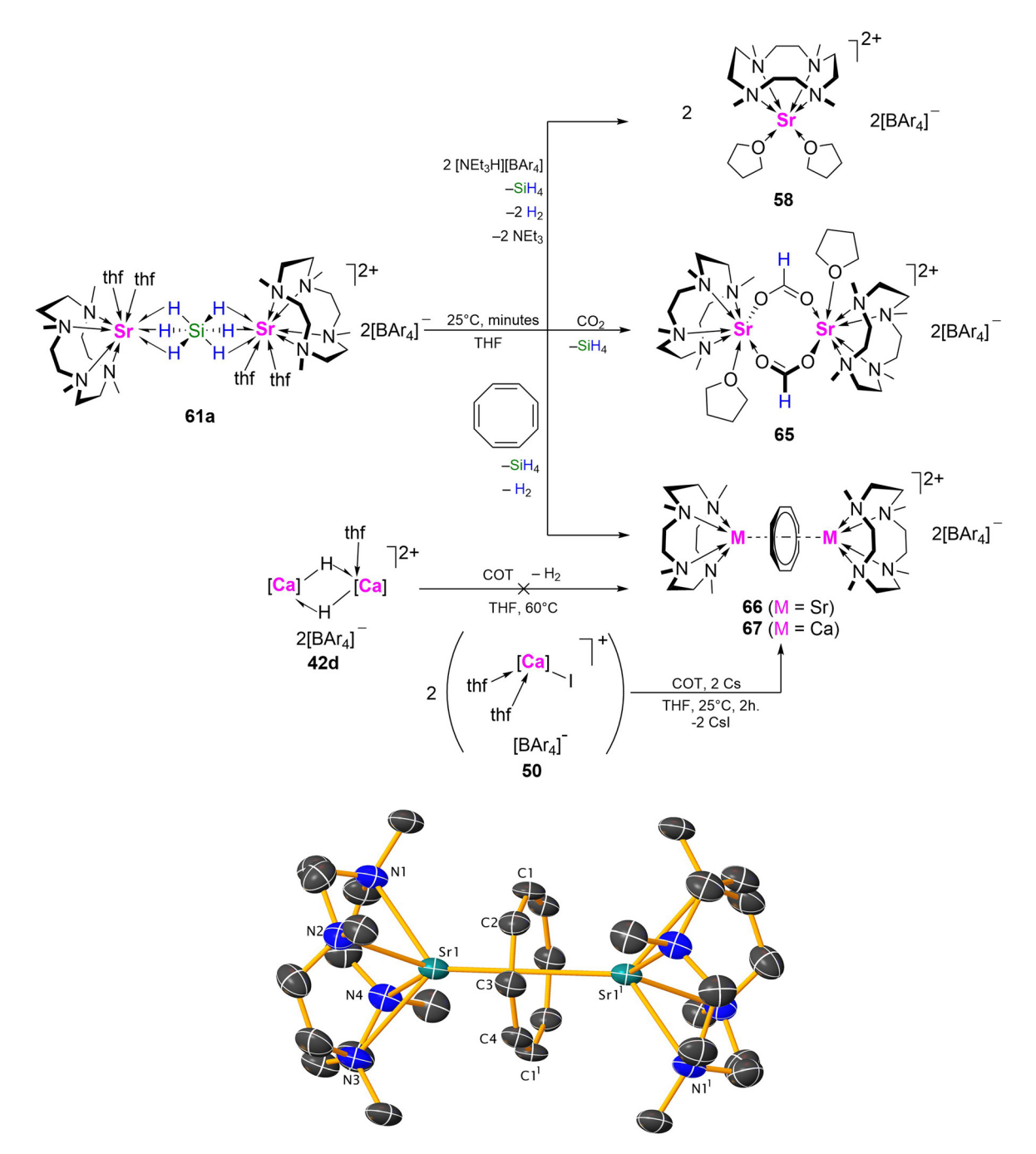
Hydrogenolysis of 68 resulted in the release of free Me₄TACD, toluene, and the precipitation of [BaH₂]_n (Scheme 26). The in situ ¹H NMR spectrum displayed a broad resonance at δ 9.4 ppm, attributed to soluble oligomeric barium hydride clusters. Hydrogenolysis of 69 resulted in the formation of the THF insoluble dimeric dihydride cation $[(Me_4TACD)_2Ba_2(\mu-H)_2(thf)_4][B(C_6H_3-3,5-Me_2)_4]_2$ (70), which crystallised directly from the reaction mixture (Scheme 26). Complex 70 represents a rare crystallographically characterised molecular barium hydride. Heptanuclear and tetradecanuclear clusters $[Ba_7H_7(N(SiMe_3)_2)_7] \cdot 2C_6H_6$ and $Ba_{14}H_{12}N$ $(SiMe_3)_2$ ₁₂{ $(Me_3Si)(Me_2SiCH_2)N$ ₄] were also structurally characterised.88 The only other examples of dinuclear species are $[(Tp^{Ad,iPr})_2Ba_2(\mu-H)_2](Tp^{Ad,iPr} = hydrotris(3-adamantyl-5-iso$ propyl-pyrazolyl)borate)⁸⁹ and $[(\eta^5-C_5R_5)_2Ba_2(\mu-H)_2(DABCO)]$ (R = C₆H₃-3,5-ⁱPr),⁷¹ which are supported by extremely bulky 5-electron donor L₂X-type ligands. Although insolubility precluded characterisation of 70 by NMR spectroscopy, the crystal structure reveals the dicationic part to consist of two eightcoordinate barium centres each bound to the κ^4 -Me₄TACD, two μ-hydrides, and two THF molecules (Fig. 9). The higher coordination number compared to that of the lighter metals in 60 and 42 reflects the large size of the Ba2+ cation and its tendency to adopt higher coordination geometries.

The isolation of the barium hydride **70** is notable given the extreme lability and inaccessibility of the putative strontium congener $[(Me_4TACD)_2Sr_2(\mu-H)_2(thf)_x]^{2+}$. Its isolation, likely aided by its insolubility, prevents ligand redistribution in solu-

tion. Given the success in employing the large 15-membered *NNNNN* macrocycle Me_5PACP to strontium, 52,53 and the oftenhigher activity of barium catalysts compared to the lighter group 2 elements, 58,71,76,77,86 soluble complexes with $[Ba_2H_2]^{2+}$ moiety supported by large aza-macrocycles may be of interest. Indeed, preliminary results suggest that a soluble molecular barium hydride can be accessed by hydrogenolysis of a benzyl barium cation supported by a very large 18-membered NNNNNN macrocycle, $[(Me_6HACO)Ba(CH_2Ph)][B(C_6H_3-3,5-Me_2)_4]$ $(Me_6HACO = N,N',N'',N''',N'''',N''''-hexamethyl-1,4,7,10,13,16-hexaazacyclooctadecane), although isolation and characterisation of the proposed hydride product remains unrealised. <math>^{90}$

5. Group 12 metals

Although part of the d-block, zinc is considered a main-group element due to the stable closed-shell 3d10 electronic configuration. While zinc(II) shares some chemical similarities with magnesium(II), its higher electronegativity and increased covalent contributions lead to notable differences. Whilst no Me4TACD complexes of highly toxic cadmium and mercury are known to date, the solution-state binding of Me₄TACD to Zn²⁺ and Cd2+ as aqueous nitrate salts has been studied alongside other aza-macrocyclic ligands. 91,92 The steric and coordinative demand of Me₄TACD on the relatively small Zn²⁺ cation (fivecoordinate effective ionic radius 0.68 Å)93 is such that the invariably five-coordinate metal centre is coordinatively oversaturated. The fifth coordination site is occupied by a Lewisbasic L-type ligand in a dicationic complex or by an X-type ligand (X = halide, hydride) in a monocationic complex. [(Me₄TACD)ZnX][HBPh₃] salts are active catalysts in the hydro-



Scheme 25 Reactivity of hexahydridosilicate complex 61a to give bis(borate) 58, formate 65, and cyclooctadienyl complex 66. For comparison, calcium hydride 42d is unreactive towards 1,3,5,7-cyclooctadiene; calcium cyclooctadienyl complex 67 is accessed from iodide 50 via caesiummediated reduction and salt-metathesis. Dicationic part of the crystal structure of complex 66. Ar = C₆H₆-3,5-Me₂.

boration and hydrosilylation of polar organic substrates, and the [(Me₄TACD)ZnH]⁺ cation displays hydride-centred nucleophilicity towards electrophilic CO₂. The resolute coordinative saturation, however, restricts more complex metal-centred reactivity compared to heavier alkaline-earth derivatives or related $[L_n ZnX]^+$ cations supported by di- and tridentate ligands. Me4TACD has also recently been employed as a ligand for dizinc(1) complexes.

5.1. Zinc(π)

All crystallographically characterised Me₄TACD zinc complexes reported to date adopt a distorted square pyramidal geometry within a five-coordinate (di)cation structure. Complexation of zinc dihalides with Me₄TACD in THF leads to auto-ionisation, forming charge-separated salts [(Me₄TACD)ZnX]X (71a, X = Cl; 71b, X = Br; 71c, X = I), in high yields (Scheme 27). 94 Anion

Dalton Transactions

Scheme 26 Synthesis of barium benzyl complexes 68 and 69 and their respective hydrogenolysis to give BaH₂ and 70. Ar = C_6H_6 -3,5-Me₂.

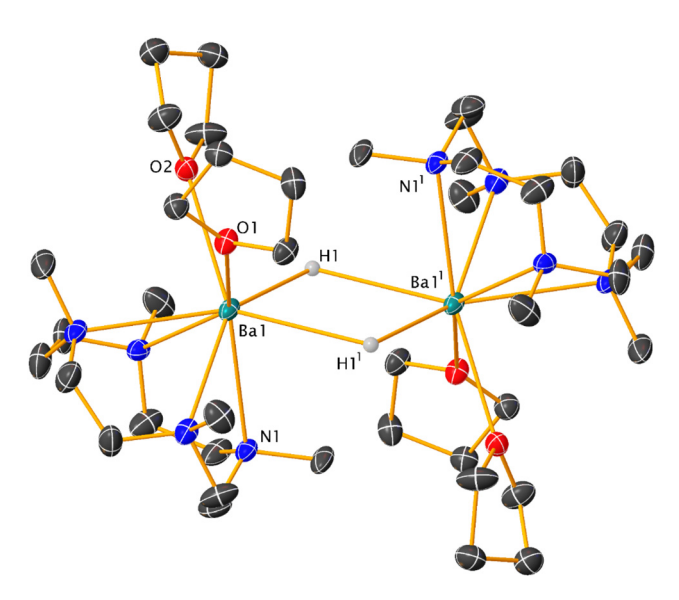


Fig. 9 Dicationic part of the crystal structure of barium hydride 70 with hydrogen atoms omitted except for barium-bound hydrides.87

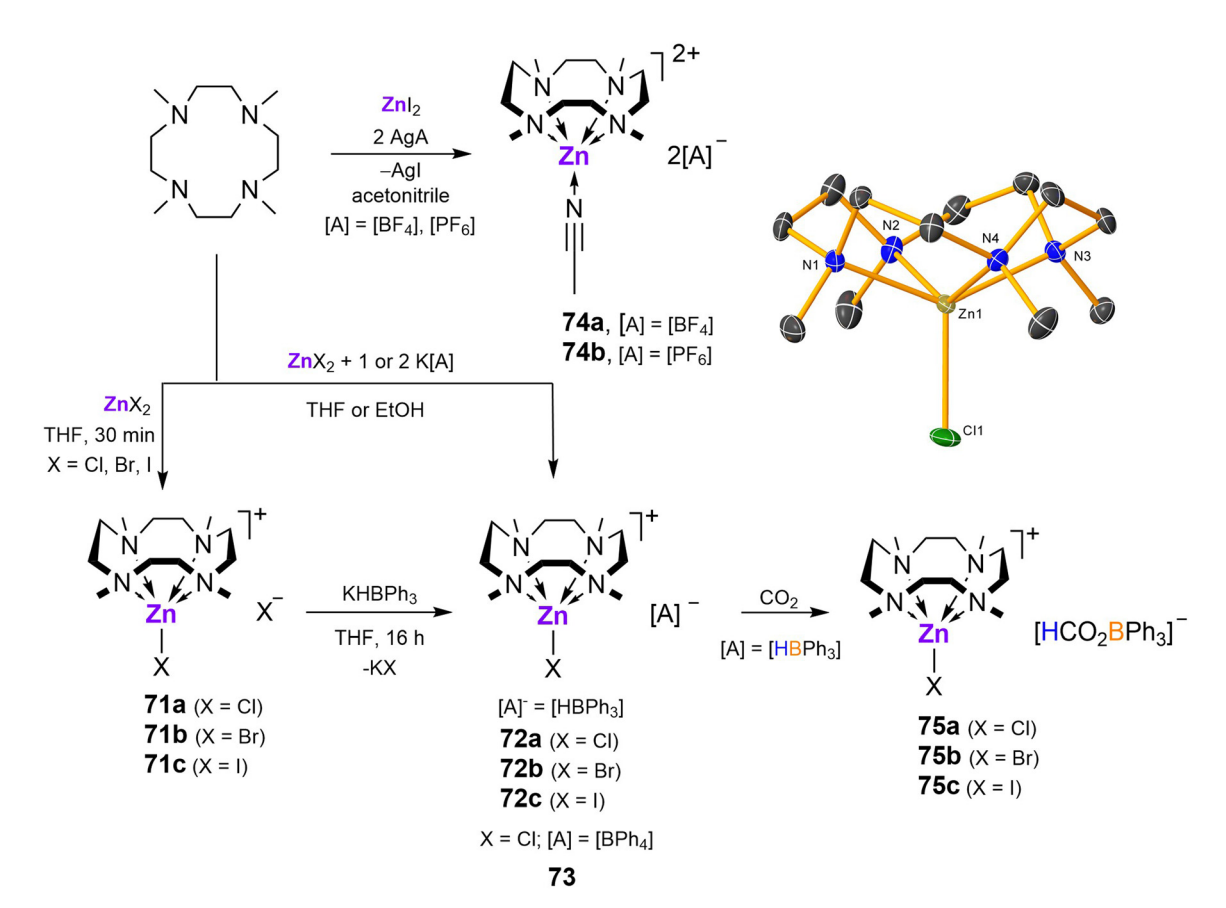
exchange with Na[BPh4] or K[HBPh3] provided access to cationic halide complexes [(Me₄TACD)ZnX][HBPh₃] (72a, X = Cl; 72b, X = Br; 72c, X = I)⁹⁴ and $[(Me_4TACD)ZnCl][BPh_4] (73)^{95}$ in high yields (Scheme 27). A two-fold halide abstraction was carried out by reacting Me₄TACD with ZnI₂ and two equiv. Ag [BF₄] or Ag[PF₆] in one pot, yielding dicationic acetonitrile complexes $[(Me_4TACD)Zn(NCCH_3)][A]_2$ (74a, $[A] = BF_4$; 74b, [A]= PF₆; Scheme 27). 96 Compounds 73 and 74 were employed as diamagnetic diluents in magnetic relaxation studies of isostructural Cu(II) congeners. 95-97 Hydridotriphenylborate complexes 72a-c react with CO₂ via insertion into the H-B bond to provide formatotriphenylborate salts $[(Me_4TACD)]$ $ZnX[HCO_2BPh_3]$ (75a, X = Cl; 75b, X = Br; 75c, X = I; Scheme 27).94

Cationic amido zinc complex [(Me₄TACD)Zn (N(SiMe₂H)₂)][HBPh₃] (72d) was prepared by BPh₃ mediated hydride abstraction of $[Zn(N(SiMe_2H)_2)_2]_2$ in the presence of Me₄TACD, with elimination of the cyclic silazane [(Me₂HSiN)₂(SiMe₂)₂] (Scheme 28).⁹⁴ Like its halide analogues, 72d reacts with CO2 through rapid insertion into the B-H forming formatoborate [(Me₄TACD)Zn bond, salt $(N(SiMe_2H)_2)[HCO_2BPh_3]$ (75d).

Zinc dihydride [ZnH₂]_n does not react with Me₄TACD alone but reacts with Lewis acids in the presence of neutral N-donors to provide molecular complexes. Reaction of $[ZnH_2]_n$ with Me₄TACD in the presence of BPh₃ yields a five-coordinate zinc hydride cation [(Me₄TACD)ZnH][HBPh₃] (76a; Scheme 29). 98 A similar, four-coordinate charge-separated species [(PMDTA) ZnH][HBPh3] was obtained using tridentate PMDTA, but bidentate N-donors provide four-coordinate dihydrides [(L)Zn (H)(μ_2 -H)BPh₃], with a μ_2 -hydride bridging the zinc and boron centres.⁹⁸ The cationic zinc hydride cation was also obtained as tetraarylborate salts, $[(Me_4TACD)ZnH][BAr_4]$ (Ar = C_6H_3 -3,5- Me_2 (76b), C_6H_3 -3,5-(CF_3)₂ (76c)) by combining zinc dihydride with Brønsted acidic [(Me₄TACD)H][BAr₄] in THF. 99

CO₂ rapidly inserts into both B-H and Zn-H bonds of 76a to provide charge-separated zinc formate-formatoborate complex $[(Me_4TACD)Zn(\kappa O-OCHO)][(OCHO)BPh_3]$ (77a), 98 or into the Zn-H bond of 76b to form formatozinc cation $[(Me_4TACD)Zn(\kappa O-OCHO)][BAr_4]$ (77**b**; Scheme 29). 99 The terminal formate ligand in 77a and 77b binds zinc in a κO manner. The direct reaction of $[ZnH_2]_n$ with CO_2 in the presence of Me₄TACD yielded the charge-separated diformate [(Me₄TACD) Zn(κO-OCHO)[[OCHO] (77c), unlike acyclic bi- and tri-dentate polyamines, which form monomeric diformate complexes $[(L_n)]$ $Zn(OCHO)_2$ (L_n = TMEDA, TEEDA, TMPDA, PMDTA).⁹⁸

Compound 76b also reacts with BH3:thf to form the mononuclear tetrahydridoborate [(Me₄TACD)Zn(μ-H)₂BH₂][BAr₄] (78, Ar = C_6H_3 -3,5-Me₂).⁹⁹ The η^2 binding mode of the tetrahydrido-



Scheme 27 Complexation of zinc dihalides by Me_4TACD , anion-exchange derivatives, and reactivity of hydridoborate derivatives towards CO_2 . Cationic part of the crystal structure of compound 73 (H-atoms omitted).

Scheme 28 Synthesis of amidozinc hydridoborate complex, and its reactivity towards CO₂.94

borate moiety in 78 contrasts to the η^3 -coordinated tetrahydridoborate in the congeneric magnesium complex 24.⁴⁷

5.1.1. Catalysis mediated by [(Me₄TACD)ZnX][HBPh₃] complexes. Zinc [HBPh₃]⁻ derivatives were employed as catalysts for hydrofunctionalisation of polar substrates (Table 1). Complexes **72a–d** were tested for hydroboration of ketones, imines, esters, amides, pyridine, and CO₂ using HBpin as hydride source.⁹⁴ The amide derivative **72d** exhibited the highest activity, readily hydroborating benzophenone, benzimine, and pyridine under mild conditions, although alkaliand alkaline-earth derivatives were more active.^{36,100} CO₂ was reduced to MeOBpin and pinBOBpin in 16 h at 60 °C. Complex **76a** catalyses selective CO₂ hydrosilylation to formate

using n-butyldimethylsilane as hydride source. ⁹⁸ The silylformate was obtained in quantitative spectroscopic yields with 5 mol% **76a** at 70 °C under 1 bar CO_2 in 48 h. Although silane conversion occurred as quickly as with bi- and tri-dentate derivatives, methoxysilane formation was minimal for the tetradentate macrocycle due to the oversaturation of the five-coordinate zinc centre.

The tetraarylborate derivative 76b is inactive in the hydrosilylation of CO_2 . Crystals of the zinc formate-hydridoborate salt $[(Me_4TACD)Zn(\kappa O\text{-}OCHO)][HBPh_3]$ (77d, Fig. 10) were obtained from a concentrated reaction solution of the hydrosilylation of CO_2 with n-butyldimethylsilane and catalyst 77a, which may imply that the zinc formate cation is itself incap-

Scheme 29 Reaction of $[ZnH_2]_n$ with Me_4TACD in the presence of Lewis acids BPh_3 or CO_2 , reaction of $[ZnH_2]_n$ with $[(Me_4TACD)H]^+$, and onward reactivity of hydridozinc cations toward CO_2 and BH_3 -thf. 98,99 Crystal structure of compound 77a (H-atoms omitted except for H1 and H14). 98

able of turnover.⁹⁹ Notably, zinc hydride cations $[(L_n) \text{ZnH}][\text{BAr}_4]$ supported by acyclic ligands $(L_n = \text{TMEDA}, \text{TEEDA}, \text{PMDTA}, \text{Me}_6\text{TREN}; \text{Ar} = \text{C}_6\text{H}_3\text{-}3,5\text{-}(\text{CF}_3)_2)$ are far more active in the catalytic hydrosilylation and hydroboration of CO_2 . Thus, combined hydricity and Lewis acidity is essential for active catalysis; the steric and coordinative demand of the strongly chelating Me_4TACD macrocycle quenches Lewis acidity and coordinative availability of the zinc centre and precludes zinc-mediated catalysis.

5.2 **Zinc(1)**

The unsymmetrical dizinc(1) cation [Cp*ZnZn(Me₄TACD)][BAr₄] (79; Ar = C_6H_3 -3,5-Me₂), synthesised from $[Cp_2^*Zn_2]$ and $[(Me_4TACD)H][BAr_4]$ under elimination of Cp*H (Scheme 30), 103 is unreactive towards further equivalents of $[(Me_4TACD)H][BAr_4]$. The dizinc(1) dication $[(Me_4TACD)_2Zn_2]^{2+}$ was instead accessed by reacting 79 with HBpin, providing $[(Me_4TACD)_2Zn_2][BAr_4]$ (80) in 30% yield (Scheme 30). The Zn-Zn bond in 79 is somewhat longer (2.3510(3) Å) compared to that in $[Zn_2Cp_2^*]$ (2.302(1) Å), whilst 80 shows an elongated Zn-Zn bond of 2.4860(6) Å, significantly longer than those in analogous $[Zn_2L_6]^{2+}$ dications (2.36–2.41 Å; L = THF, DMAP). 104,105

Compound 79 mediates the heterolysis of activated C-H bonds in N=CCH₃ and PhC=CH in the presence of catalytic Me₄TACD (10 mol%) as a Brønsted base, providing organozinc (II) complexes [(Me₄TACD)ZnR][BAr₄] (81a, b; R = H₂CC=N, C=CPh; Scheme 31). 103

6. Group 13 metals

Protonolysis of organo- and hydrido-triel precursors with tetraaryl borate salts of $[(Me_4TACD)H]^+$ yielded (di)cationic hydride complexes $[(Me_4TACD)AlH_2]^+$ and $[(Me_4TACD)MH]^{2+}$ (M = Al, Ga), and univalent cations $[(Me_4TACD)M]^+$ (M = Ga, In, Tl). The small ionic radius of Al^{3+} and Ga^{3+} resulted in an unusual, folded ligand conformation for $[(Me_4TACD)AlH_2]^+$ and Brønsted acidic reactivity of the Ga–H bond for coordinatively saturated $[(Me_4TACD)GaH]^{2+}$. The acid–base chemistry of the Ga(I)–(III) couple was studied.

6.1. Aluminium

The dihydridoaluminium cation [(Me₄TACD)AlH₂][BAr₄] (**82a**, Ar = C_6H_3 -3,5-Me₂; **82b**, Ar = C_6H_3 -3,5-(CF₃)₂) was synthesised in near quantitative yields by reacting Et₃N·AlH₃ with [(Me₄TACD)H][BAr₄] (Scheme 32).²⁸ The macrocyclic ligand in

recatalyst (loading), reducing agent	Substrate	Products
N N N The second seco	Ph Ph	Ph H Ph
$N_{\rm e_2HSi}$ $N_{\rm SiHMe_2}$ $72d$ $(10 {\rm mol}\%)$	CO_2	Bpin Bpin +
→ B → H		Bpin CH ₃
	PhN 	Ph _N Bpin ↓
	H Ph	H Ph
	N	H N-B
		Bpin
N N N The N	CO_2	H O Si n
(5 mol%)		

82 adopts a rare *syn-syn-syn-anti* configuration in both solid and solution states, with one methyl group pointing towards the distal face of the complex, away from the metal centre.

The crystal structure of **82b** reveals a slightly distorted *mer*-octahedral geometry, with the two hydride ligands *cis* to one another (Fig. 11). Due to macrocyclic strain, the Al1–N1 distance (2.466(3) Å) is significantly longer than the other Al–N distances (2.091(3), 2.096(3), 2.145(3) Å), with NBO analysis indicating a low Wiberg Bond Index (WBI) for this Al–N interaction compared to the others. This folded conformation was previously observed only as a minor crystalline component in

the solid-state structure of 27, which exists in an exclusively all-syn conformation in solution. Tomplex 82 represents the steric limit of the 12-membered macrocycle in chelating a small ion (effective ionic radius for six-coordinate aluminium, 0.535 Å) whilst accommodating two hydride ligands. The related 14-membered macrocycle Me₄cyclam reacts with Me₃N·AlH₃ by auto-ionization to form [(Me₄cyclam) AlH₂][AlH₄], which adopts an octahedral *trans*-dihydride motif with the larger macrocycle encircling the equatorial plane. The folded ligand conformation of 82 is retained in solution up to 60 °C, as evidenced by Th NMR spectroscopy showing a

Dalton Transactions Perspective

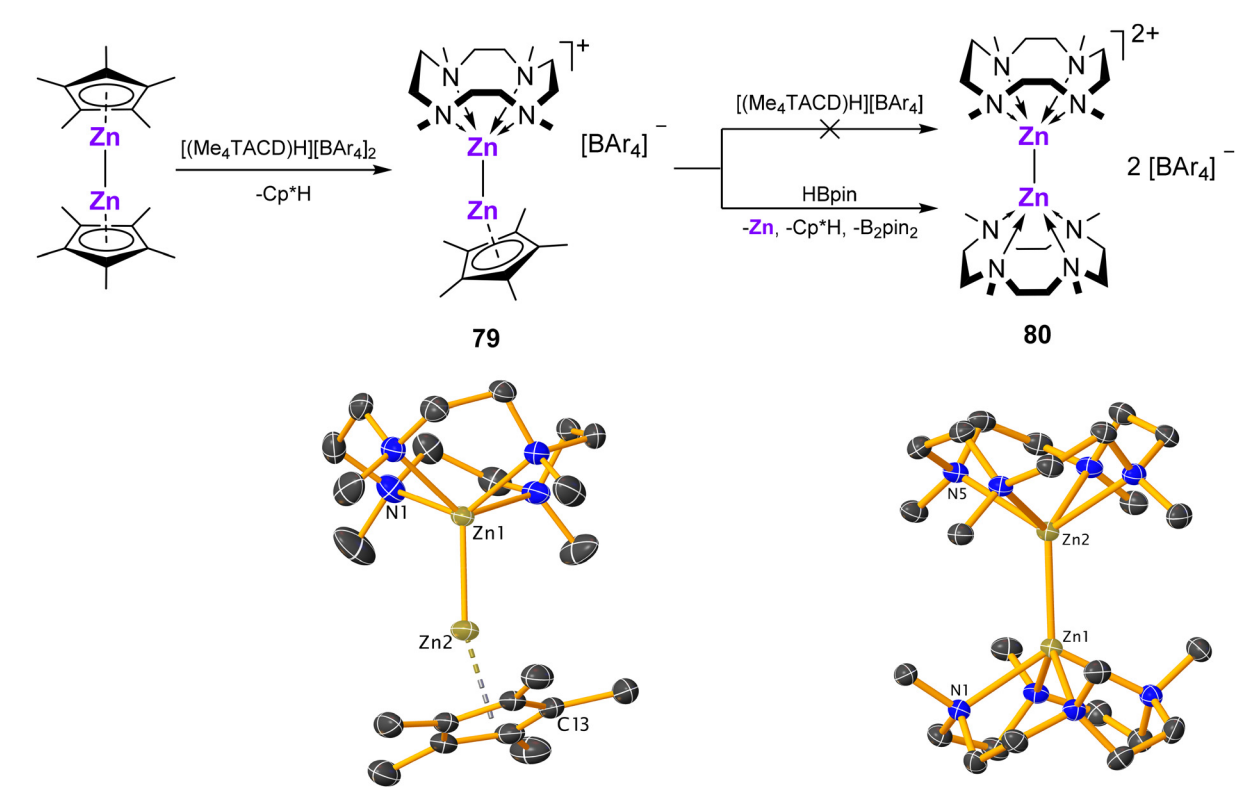
Fig. 10 Zinc formate hydridotriphenylborate 77d, isolated from the catalytic reaction mixture of CO₂ hydrosilylation by ⁿBuMe₂SiH catalysed by 76a.

complex array of multiplets corresponding to four pairs of magnetically inequivalent methylene protons, and three methyl environments in a 1:2:1 integral ratio.

Complex 82 reacts with the weak Brønsted acid [Et₃NH][BAr₄], yielding the dicationic hydride complexes [(Me₄TACD) $AlH[BAr_4]_2$ (83a, Ar = C_6H_3 -3,5- Me_2 ; 83b, Ar = C_6H_3 -3,5- $(CF_3)_2$; Scheme 33).28 1H NMR spectra confirmed that upon removal of one hydride, the macrocycle reverts to a time-averaged C₄-symmetric boat-like conformation. Depending on the counter-ion, the methylene environments in THF- d_8 appear either as a broad, unresolved signal (Ar = C₆H₃-3,5-Me₂), or a well-defined AA'XX' multiplet (Ar = C_6H_3 -3,5-(CF_3)₂), suggesting non-negligible ion pairing for the non-fluorinated anion. Compound 83 was also obtained via protonolysis of tetrameric aluminium(1) reagent [Cp*Al]₄ with [(Me₄TACD)H][BAr₄] at 70 °C (Scheme 33).²⁸ Due to the formation of a bis-borate salt, eight equivalents of conjugate acid were required to achieve quantitative conversion to an equimolar mixture of Me₄TACD, Cp*H, and 83. Four equiv. of conjugate acid resulted in the incomplete conversion of the aluminium(1) reagent. The reaction of [(Me₄TACD)H][BAr₄] with [Cp*Al] leads to protonation of the Cp* ligand, forming Cp*H, and formal two-electron oxidation of Al(1) to Al(111) hydride dication. The reaction likely proceeds via protonation of transient [(Me₄TACD)Al]⁺. Isolable mononuclear aluminium(1) cations remain elusive, but the related tetranuclear monovalent cluster cation $[(\kappa^3\text{-Me}_3\text{TACN})\text{Al}\{\kappa^3\text{-}(\text{AlCp}^*)_3\}][\text{Al}(\text{OR}^F)_4]$ (OR^F = OC(CF₃)₃), has been reported.107

6.2. Gallium

Unlike Et₃N·AlH₃, protonolysis of Me₃N·GaH₃ with equimolar $[(Me_4TACD)H][B(C_6H_3-3,5-(CF_3)_2)_4]$ yielded gallium(I) cation $[(Me_4TACD)Ga][B(C_6H_3-3,5-(CF_3)_2)_4]$ (84a, Scheme 34),²⁸ which likely forms through spontaneous dehydrogenation of a shortlived gallium(III) dihydride cation [(Me₄TACD)GaH₂]⁺. The spontaneous dehydrogenation of transient base-free [GaH2]+ has also been described. 108 Consistent with higher stability of the gallium(1) cation compared to its lighter congener, [(Me₄TACD) $Ga[B(C_6H_3-3,5-Me_2)_4]$ (84b) was synthesised via protonolysis of [Cp*Ga] with $[(Me_4TACD)H][B(C_6H_3-3,5-Me_2)_4]$ (Scheme 34).²⁸ Subsequent protonation of **84b** with [Et₃NH][B(C₆H₃-3,5-Me₂)₄] provided the dicationic hydride [(Me4TACD)GaH][B(C6H3-3,5-Me₂)₄]₂ (85) after release of triethylamine (Scheme 34).²⁸ This



Scheme 30 Synthesis of dizinc(i) complexes 79 and 80 and the (di)cationic part of their crystal structures (H-atoms omitted). 103 Ar = C_6H_3 -3,5-Me₂.

Perspective **Dalton Transactions**

Scheme 31 Reaction of dizinc(ı) compound 79 with acetonitrile and with phenylacetylene. Ar = C_6H_3 -3,5-Me₂.

observation is consistent with the protonation of proposed [(Me₄TACD)Al]⁺ in the synthesis of 83 from [Cp*Al]₄. Similar protonation with oxidative addition of H-P bond to [Ga]+ was reported in the reaction of [(PhF)_nGa][Al(OR^F)₄] with [HPPh₃][Al (OR^F)₄] in the presence of triphenylphosphine. ¹⁰⁹

Scheme 32 Synthesis of aluminium hydrides 82a,b.

The gallium(1) cation 84 forms a charge-separated ion-pair in the solid-state, with a four-coordinate gallium cation and a pseudo C₄-symmetric macrocyclic ligand (Fig. 12a).²⁸ The Ga-N distances are notably shorter than the Ga-O distances in the related [(12-crown-4)Ga][A] (A = $[GaCl_4]^-$, $[B(C_6F_5)_4]^-)^{110}$ and the metal centre projected less from the basal plane of the four donor atoms. 84 is formally isoelectronic to the germanium dication of $[(Me_4TACD)Ge]X_2$ (90a, $X = CF_3SO_3^-$; 90b, X =GeCl₃⁻) (vide infra), which displays significantly shorter M-N bonds due to the higher nuclear charge of the tetrel dication. 111 The 1H NMR spectrum confirms stable macrocycle coordination, displaying a resolved methylene AA'XX' spin system at room temperature. The ⁷¹Ga NMR spectrum (122 MHz, 298 K) of 84 contains a broad signal at δ –173 ppm (84b, acetonitrile- d_3) or -188 ppm (84a, THF- d_8), significantly downfield-shifted compared to Ga[Al(ORF)₄] coordinated by arene or fluoroarene solvents (δ –756 ppm, C₆H₅F; –520 ppm, $(C_7H_8)^{112}$ or ethers $(\delta -448 \text{ ppm, } Ga[Al(OR^F)_4] \text{ in } THF;^{112}$

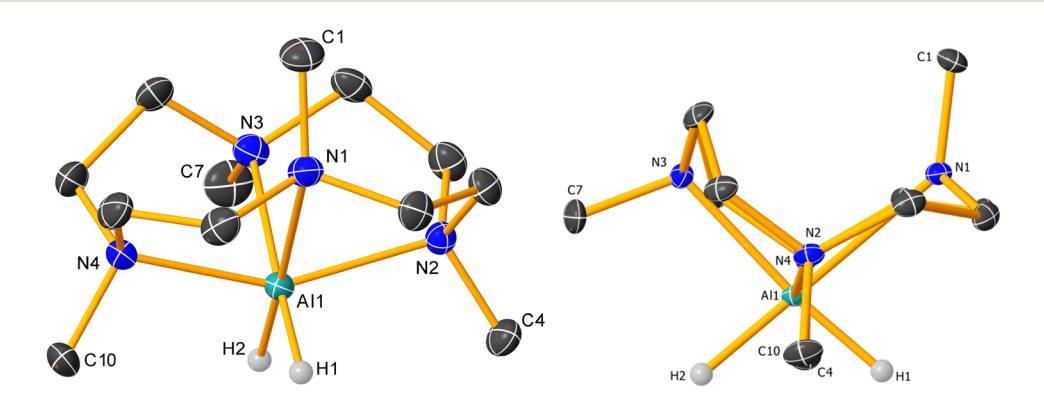
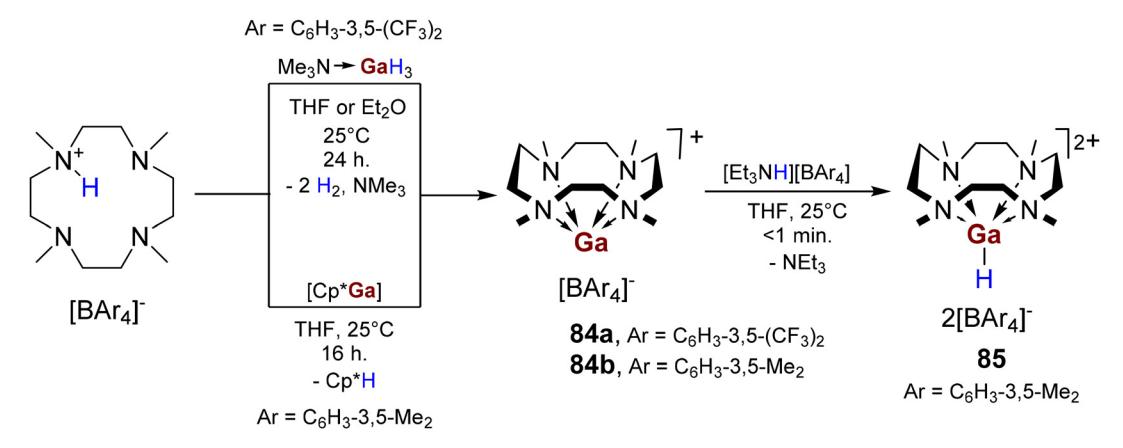


Fig. 11 Crystal structure (H-atoms omitted except H1 and H2) of the cationic part of the of 82b in oblique (left) and side (right) views.²⁸

$$\begin{bmatrix} Et_3NH][BAr_4] \\ H \\ H \\ \end{bmatrix} \begin{bmatrix} Et_3NH][BAr_4] \\ THF \\ -H_2, NEt_3 \\ \end{bmatrix} \begin{bmatrix} N \\ AI \\ N \\ \end{bmatrix} \begin{bmatrix} N \\ N \\ \end{bmatrix} \begin{bmatrix} THF, 50^{\circ}C \\ 3-24 \text{ h.} \\ -Cp^{\circ}H \\ -Me_4TACD \\ \end{bmatrix} \begin{bmatrix} BAr_4 \end{bmatrix}^{-} \begin{bmatrix} BAr_4$$

Scheme 33 Synthesis of aluminium hydride dication 83a,b from protonolysis of 82a,b, or protonolysis-protonation of [Cp*Al]4.

Dalton Transactions Perspective



Scheme 34 Synthesis of gallium(i) complexes 84a,b by protonolysis/dehydrogenation of Me₃N·GaH₃ or protonolysis of [Cp*Ga]; synthesis of gallium(iii) hydride dication 85.

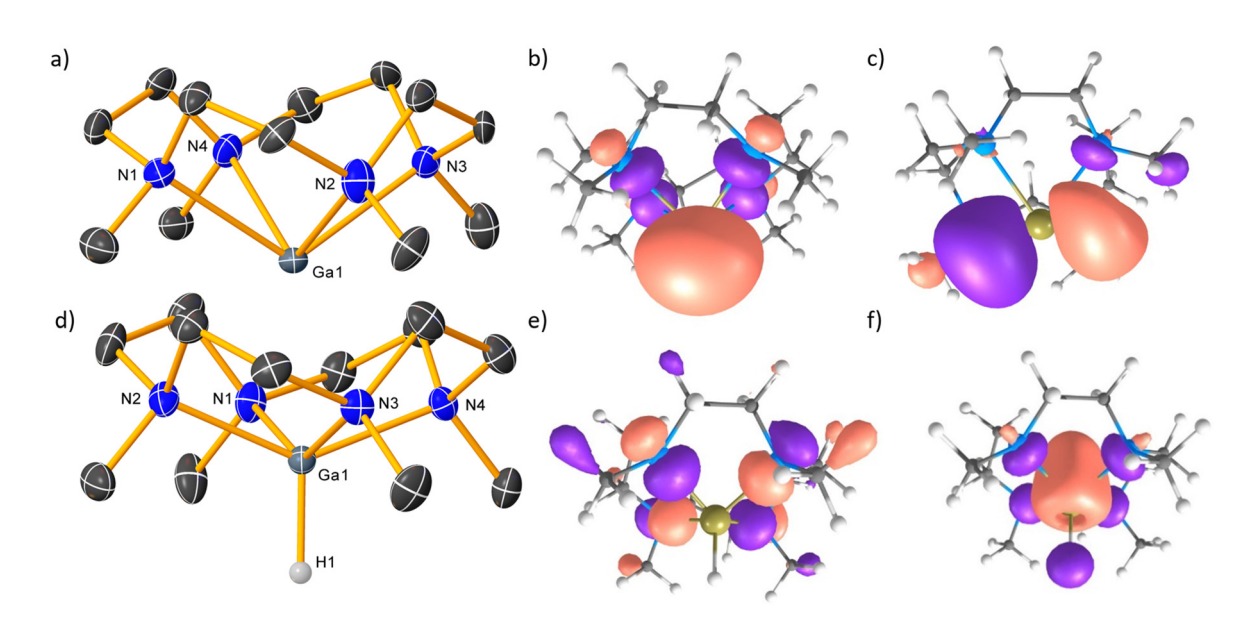


Fig. 12 Crystal structures (H-atoms omitted except for the gallium-bound hydride) of the (di)cationic parts from (a) 84b; (b) calculated HOMO, and (c) LUMO of $[(Me_4TACD)Ga]^+$; (e) calculated HOMO, and (f) LUMO of $[(Me_4TACD)GaH]^{2+}$.

-471 ppm, [(12-crown-4)Ga][GaCl₄] in toluene). ¹¹⁰ Unlike **84**, the ¹H NMR spectrum of [(Me₃TACN)Ga][Al(OR^F)₄]¹⁰⁷ shows a single broad singlet for the methylene protons and no detectable ⁷¹Ga resonance, suggesting ligand lability. In the crystal structure of **85** (Fig. 12d), the metal centre adopts a square pyramidal geometry ($\tau_5 = 0.03$) with a terminal hydride in the apical position. Reflecting the higher formal oxidation state of +3, the Ga–N bonds are contracted by 0.33 Å, and the metal is pulled much closer to the basal N₄-plane compared to [(Me₄TACD)Ga]⁺.

The macrocycle size and the nature of donor atoms significantly impact the frontier molecular orbitals of $[(L_n)Ga]^+$. NBO analysis of **84** revealed a HOMO comprising of an out-of-phase combination of a metal-localized lone pair and Ga–N σ -bonds, while the LUMO is an empty 4p orbital (Fig. 12b and c). [12-crown-4)Ga]⁺ displayed a similar directional lone pair (HOMO)

and p-like LUMO, but the weaker donor properties of the crown-ether resulted in a lower energy HOMO compared to 84. This suggests reduced reactivity, though no experimental studies have confirmed this effect. The 18-crown-6 complex cation [(18-crown-6)Ga]⁺ displays a non-directional lone-pair that is only slightly influenced by weakly bound axial solvent molecules, owing to near-coplanarity of the larger macrocycle and metal centre. 113-115 On account of a stabilised ns-orbital, "naked" Ga⁺ and In⁺ cations, ligated by weaklybound solvent molecules and supported by weakly-coordinating anions react as oxidants and soft Lewis acids. 116-118 Coordination of σ-donor ligands raises the energy of the HOMO, leads to a directional lone-pair, and promotes reductive chemistry but often leads to disproportionation into zeroand trivalent products. 109,110,119-123 The Me4TACD ligand leads to activation of the 4s orbital, leading to Brønsted basic reactivPerspective **Dalton Transactions**

ity towards [Et₃NH]⁺ whilst imparting remarkable kinetic stability to the monovalent cation; 84b is stable up to at least 60 °C in THF. No oxidation event could be determined for 84b by cyclic voltammetry up to +1.1 V (vs. Fc/Fc⁺ in acetonitrile), but an irreversible reduction at -2.5 V was tentatively ascribed to the Ga^{I}/Ga^{0} couple. 124 $[Ga(o-C_{6}H_{4}F_{2})_{n}][Al(OR^{F})_{4}]$ gives a scanrate dependent, partially reversible event at about +3.0 V (Ga^I/ $Ga^{0} \nu s. Fc/Fc^{+} in o-C_{6}H_{4}F_{2}).^{116}$

NBO analysis of 85 showed that its HOMO (Fig. 12e) is primarily composed of Ga-N bonding orbitals, while the LUMO is dominated by the Ga-H σ^* antibonding orbital (Fig. 12f).²⁸ Accordingly, 85 is readily deprotonated at room temperature by IMe₄ (1,3,4,5-tetramethyl-imidazol-ylidene) to return to 84b and eliminate the imidazolium salt [IMe₄H][B(3,5-Me₂-C₆H₃)₄] (Table 2). Treating 85 with equimolar DBU (1,8-diazabicyclo [5.4.0]undec-7-ene, $pK_a(CH_3CN) = 24.3$) resulted in an equilibrium mixture of conjugate acid-base pairs, which allows estimation of the Brønsted acidity of the gallium hydride as $pK_a(CH_3CN) = 24.5$ using NMR spectroscopy. Brønsted acidity is appreciable for heavier tetravalent group 14 hydrides, 4,125,126 but the reactivity of group 13 hydrides is normally characterised by strong Brønsted basicity and nucleophilicity. Brønsted acidity is more reminiscent of late-transition metal hydrides.

Unlike isoelectronic $[(Me_4TACD)ZnH]^+$ (76a,b), which rapidly inserts CO₂ to give [(Me₄TACD)Zn(OCHO)]⁺ (77a,b), 85 is inert towards CO2 under ambient conditions. However, 84b reacts with CO2 (1 bar) in THF or acetonitrile solution to provide the cationic carbonate complex [(Me₄TACD)Ga(κ₂- O_2CO][B(C_6H_3 -3,5-Me₂)₄] (86) with CO extrusion (Scheme 35). This reaction likely proceeds via a putative oxido gallium cation [(Me₄TACD)GaO]⁺ through CO extrusion from a transient CO₂ complex [(Me₄TACD)Ga(CO₂)]⁺. Although [(Me₄TACD) GaO]⁺ remained elusive, oxidation of **84b** with N₂O in the presence of BPh₃ produces [(Me₄TACD)GaO·BPh₃][B(C₆H₃-3,5-Me₂)] (87), which itself reacts with CO₂ to form a gallium carbonate.

84b acts as a pre-catalyst for the CO₂ hydroboration to form pinBOC(H)O using HBpin. Although the mechanistic details remain obscure, the formation of a Me₄TACD-containing intermediate with a 1H NMR typical for gallium(III) (downfield shifted AA'XX' multiplet) and CO during catalyst activation suggests initial oxidation of 84b by CO2. 124

6.3. Indium and thallium

Similar to the synthesis of 84b, the heavier monovalent cations $[(Me_4TACD)M][B(C_6H_3-3,5-Me_2)_4]$ (8 M = In; 89, M = Tl) were prepared by protonolysis of $[Cp*M]_n$ (M = In, n = 6; M = Tl, n = 6) ∞) with [(Me₄TACD)H][B(C₆H₃-3,5-Me₂)₄] (Scheme 36).

The compounds 84, 88, and 89 are structurally similar, with metal centre moving further from the basal N₄-plane with increasing atomic number (1.3007(15) Å, 84; 1.501(2)/1.521(2) Å, 88; 1.616(5) Å, 89), with a larger increase in difference between Ga and In (ca. 0.2 Å) than between In and Tl (0.1 Å) due to the lanthanide contraction. The crystal structure of 88 is shown in Fig. 13a. Calculated Wiberg Bond Indices (WBIs) for the M-N bonds decreased down group 13, reflecting increased size- and hard-soft mismatch between ligand and metal. Alternative polydentate ligands with softer sulphur, phosphorus, and arsenic donors have been explored for the heavier group 14 elements, 127 and may be well-suited to heavy univalent group 13 cations. Indeed, acyclic monodentate and chelating phosphines have already been employed for univalent gallium and indium cations. 128-132

The ¹H NMR spectra of **88** and **89** resemble that of **84b** but lack a resolved methylene spin system. Similar signal broadening was observed for increasingly heavy alkali metal silanides, but this was attributed to the lability of the macrocycle.41 Ligand resonances in the ¹H NMR spectrum of [(Me₃TACN) Tl][Al(ORF)₄] shift on addition of excess Me₃TACN, ¹⁰⁷ indicating labile coordination to soft Tl(1) cation. However, for 88 and 89, persistent coordination is observed at elevated tempera-

Table 2 Acid-base chemistry of compounds 84a and 85. Ar = C_6H_3 -3,5- Me_2^{28}

[BAr₄] + [Base-H][BAr₄]
$$\frac{\kappa_{eq}}{\text{THF or acetonitrile}}$$
 $\frac{\kappa_{eq}}{\kappa_{eq}}$ $\frac{\kappa_{eq}}{\kappa_{eq}}$

$K_{ m eq}$	Solvent
≫1 (quantitative protonation)	THF
0.77	Acetonitrile
0 (quantitative deprotonation)	THF
	≫1 (quantitative protonation) 0.77

Dalton Transactions

Scheme 35 Reactivity of 84b and 85 towards CO₂ and N₂O (Ar = C₆H₃-3,5-Me₂). Cationic part of the crystal structure of 86 (H-atoms omitted). 124

Not isolated Proposed structure

Scheme 36 Synthesis of compounds 88 and 89.

tures as their methylene resonances split into two unresolved multiplets. At low temperatures, the time-averaged ring-twisting motion is "frozen-out", as indicated by ¹H and ¹³C NMR spectroscopy showing four inequivalent CH2 (ABMX spin system) and two inequivalent CH2 resonances indicative of a static C_4 -symmetric structure (Fig. 13b). The methyl resonances in the ¹H and ¹³C{¹H} NMR spectra of 89 appeared as doublets at room temperature, due to temperature-dependent *J*-coupling to the 205 Tl nucleus (S = 1/2), although the corresponding ²⁰⁵Tl NMR spectrum was not recorded.

Neither 88 nor 89 react with $[Et_3NH][B(C_6H_3-3,5-Me_2)_4]$, suggesting that the putative conjugate acids [(Me₄TACD)MH]²⁺ have a p $K_a(CH_3CN) \gg 18.83$ and that the univalent cations are less basic than NEt3. The lone pairs (HOMO) of 88 and 89 were calculated to reside -3.1 kcal mol⁻¹ and -23.1 kcal mol⁻¹

lower in energy than that of 84, suggesting [(Me₄TACD)InH]²⁺ to be a synthetically viable target.²⁸

Group 14 metals

Me₄TACD supported germanium dications [Ge(Me₄TACD)]X₂ (90a, $X = CF_3SO_3^-$; 90b, $X = GeCl_3^-$) were isolated as colourless solids by reacting GeCl₂(dioxane) with Me₄TACD in 1:1 and 1:3 ratios, respectively, in the presence of Me₃SiO₃SCF₃ for the former compound (Fig. 14). 111 Both compounds exist as chargeseparated ion pairs in the solid state, with no significant cationanion interactions. Whilst computational studies show that the HOMO of cryptand encapsulated Ge²⁺ dication [(222-crypt) Ge][O₃SCF₃]₂ and related [12]-crown-4 sandwich dication [([12]-

Perspective **Dalton Transactions**

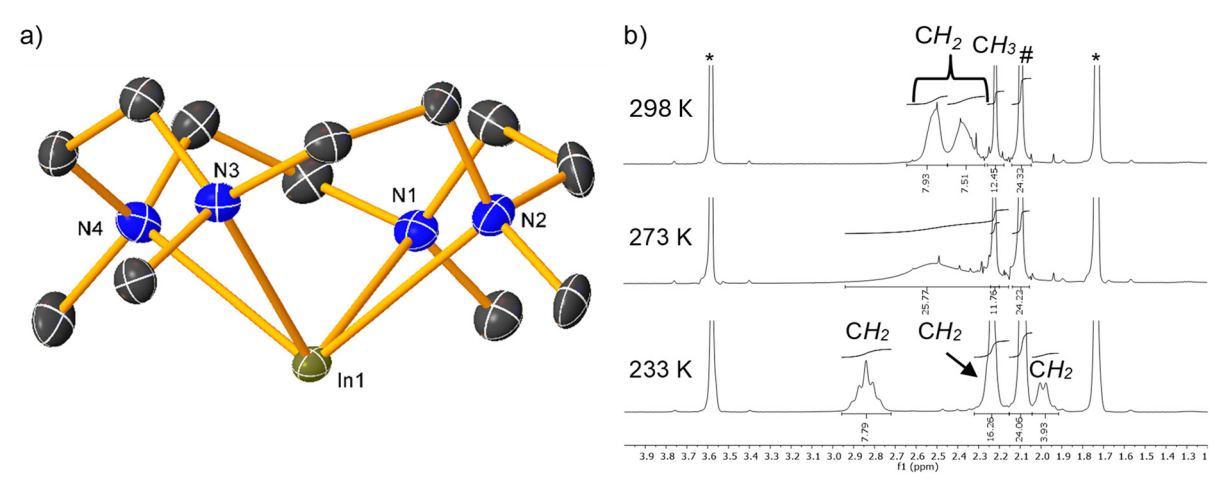


Fig. 13 (a) The crystal structure of the cationic part of 88 (30% level, H-atoms excluded); (b) stacked 1 H NMR spectra (400 MHz, THF- d_{8} (*)) of 88 at different temperatures (# borate anion).²⁸

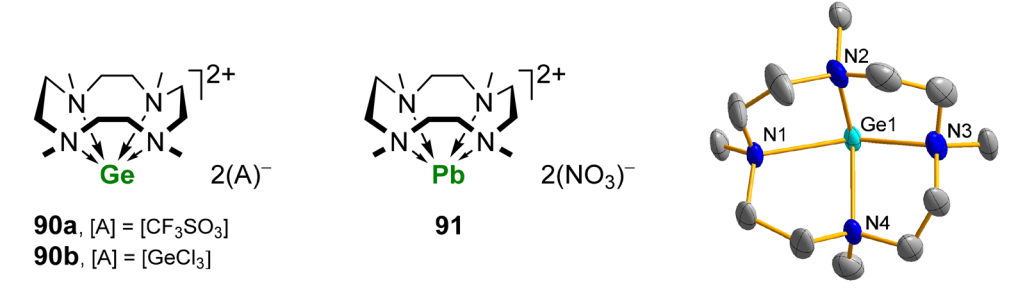


Fig. 14 Me₄TACD supported germanium and lead cations 90a,b, and 91 and the molecular structure of the cationic part of 90a. 111

crown-4)₂Ge [A]₂ ([A] = GeCl₃, O₃SCF₃) is an essentially non-directional 4s orbital, 133-135 the stronger coordinating ability of the aza-macrocycle and 'half-sandwich' structure of 90a and 90b likely induces some directionality to the 4s lone pair. This effect has been computationally demonstrated for thia-macrocycle complexes of Ge(II), 136 as well as formally isoelectronic 84 and [(12-crown-4)Ga]^{+, 28,110} Similar to **90**, the 14-membered macrocycle Me₄cyclam provides a charge-separated Ge²⁺ complex [(Me₄cyclam)Ge][GeCl₃]₂, ¹³⁴ whilst 12-membered Me₃TACN permits closer interaction with triflate and chloride anions, though bromide remains fully charge separated. 111,134

The aqueous coordination chemistry of Pb(NO₃)₂ has been studied for several aza-macrocyclic ligands, including Me₄TACD, although the resulting lead complex 91 was not structurally characterised. 91,92

8. Conclusions

The macrocycle Me₄TACD is a versatile neutral ligand that has been employed to stabilise low-nuclearity molecular complexes of various main group metals. Compared to crown ethers, it offers greater robustness against degradation by nucleophilically induced ring-opening and stronger coordination due to the superior σ -donating properties of its amine functionality.

Its inherent flexibility allows it to accommodate main group metal centres with remarkably varying ionic radii and reactive bonds such as terminal hydride. 138

Me₄TACD efficiently encapsulates small metal cations like Li⁺, Mg²⁺, Zn²⁺, Al³⁺, and Ga³⁺, leading to coordinative saturation and limiting reactivity. For example, complexes such as $[(Me_4TACD)ZnH]^+$ (ref. 98) or $[(Me_4TACD)_2Mg_2(\mu-H)_2]^{2+}$ (ref. 47) react only with highly activated polar electrophiles, but not with apolar substrates such as H2 or alkenes. On the other hand, blocking access to the metal can induce unusual chemical reactivity, such as Brønsted acidity of the gallium(III) hydride dication [(Me₄TACD)GaH]²⁺.²⁸

Predominantly electrostatic interactions with the larger and less-well encapsulated group 1 cations K-Cs lead to labile coordination of the macrocycle, as indicated by NMR spectra of the triphenylsilanide series [(Me₄TACD)MSiPh₃] (M = Li-Cs).41 Heavier monovalent group 13 cations Ga-Tl are more strongly coordinated, such that the macrocycle engenders a degree of basic and reducing reactivity to the otherwise lowlying 4s lone-pair of Ga⁺. ²⁸ The tuning of frontier molecular orbital energies is important in developing transition-metallike reactivity in low-valent p-block chemistry.

Me₄TACD effectively stabilizes cationic calcium hydride complexes, 137 where it strikes a balance between suppressing aggregation and ligand redistribution (Schlenk equilibria), and

Dalton Transactions Perspective

allowing facile access of substrates to the coordinatively unsaturated metal centre. Dimeric calcium hydrides salts $[(Me_4TACD)_2Ca_2(\mu-H)_2(thf)_x]^{2+}$ and $[(Me_4TACD)_2Ca_2(\mu-H)_3]^+$ serve as active catalysts for alkene hydrogenation and hydrosilylation. However, its ability to stabilise analogous complexes of strontium instead leads to trinuclear hydride $[(Me_4TACD)_3Sr_3(\mu-H)_4(thf)]^{2+}$ (ref. 80) and di- or trinuclear hydridosilicate species. Dimeric strontium complexes are better stabilised by the larger 15-membered NNNNN macrocycle Me₅PACP. Whilst a dimeric barium dihydride dication $[(Me_4TACD)_2Ba_2(\mu-H)_2(thf)_4]^{2+}$ has been crystallographically characterised, solution-state its chemistry remains unexplored.87

Although the elaboration of reaction chemistry and catalysis for very small or very large main group metals may be limited by respective coordinative saturation and lability, as a supporting ligand for reactive cations, Me₄TACD has the potential to offer significant opportunities in the future development of s-block mediated catalysis and low-valent p-block chemistry alongside its more widely established cousins such as Me₃TACN, crown-ethers and acyclic polyamines. We hope this review stimulates future research activity in this regard.

Author contributions

P. G., L. M. and J. O. conceptualised and wrote the manuscript.

Data availability

No primary research results, software or code have been included and no new data were generated or analysed as part of this review.

Conflicts of interest

There are no conflicts to declare.

Acknowledgements

J. O. acknowledges the Deutsche Forschungsgemeinschaft for financial support and all the former coworkers for their hard work. Professor Shigehiro Yamaguchi, Nagoya University, kindly provided facilities at the Research Center for Material Science to complete this manuscript.

References

1 C. M. Cui, H. W. Roesky, H. G. Schmidt, M. Noltemeyer, H. J. Hao and F. Cimpoesu, Angew. Chem., Int. Ed., 2000, 39, 4274-4276.

- 2 T. J. Hadlington, M. Hermann, J. Li, G. Frenking and C. Jones, Angew. Chem., Int. Ed., 2013, 52, 10199-10203.
- 3 A. S. S. Wilson, M. S. Hill, M. F. Mahon, C. Dinoi and L. Maron, Science, 2017, 358, 1168-1171.
- 4 S. Wang, T. J. Sherbow, L. A. Berben and P. P. Power, J. Am. Chem. Soc., 2018, 140, 590-593.
- 5 J. Hicks, P. Vasko, J. M. Goicoechea and S. Aldridge, Nature, 2018, 557, 92-95.
- 6 J. Hicks, P. Vasko, J. M. Goicoechea and S. Aldridge, Angew. Chem., Int. Ed., 2021, 60, 1702-1713.
- 7 P. M. Chapple, S. Kahlal, J. Cartron, T. Roisnel, V. Dorcet, M. Cordier, J.-Y. Saillard, J.-F. Carpentier and Y. Sarazin, Angew. Chem., Int. Ed., 2020, 59, 9120-9126.
- 8 B. Rosch, T. X. Gentner, J. Eyselein, J. Langer, H. Elsen and S. Harder, Nature, 2021, 592, 717-721.
- 9 R. Mondal, M. J. Evans, T. Rajeshkumar, L. Maron and C. Jones, Angew. Chem., Int. Ed., 2023, 62, e202308347.
- 10 F. Dankert, J. Messelberger, U. Authesserre, A. Swain, D. Scheschkewitz, B. Morgenstern and D. Munz, J. Am. Chem. Soc., 2024, 146, 29630-29636.
- 11 V. Nesterov, D. Reiter, P. Bag, P. Frisch, R. Holzner, A. Porzelt and S. Inoue, Chem. Rev., 2018, 118, 9678-9842.
- Arrowsmith, H. Braunschweig, M. A. Celik, Dellermann, R. D. Dewhurst, W. C. Ewing, K. Hammond, T. Kramer, I. Krummenacher, J. Mies, K. Radacki and J. K. Schuster, Nat. Chem., 2016, 8, 890-894.
- 13 M.-A. Légaré, G. Bélanger-Chabot, R. D. Dewhurst, E. Welz, I. Krummenacher, B. Engels and H. Braunschweig, Science, 2018, 359, 896-900.
- 14 P. Bag, A. Porzelt, P. J. Altmann and S. Inoue, J. Am. Chem. Soc., 2017, 139, 14384-14387.
- 15 Y. Wang and G. H. Robinson, J. Am. Chem. Soc., 2023, 145, 5592-5612.
- 16 J. L. Dye, Philos. Trans. R. Soc., A, 2015, 373, 20140174.
- 17 S. D. Robertson, M. Uzelac and R. E. Mulvey, Chem. Rev., 2019, 119, 8332-8405.
- 18 N. Davison, P. G. Waddell and E. Lu, J. Am. Chem. Soc., 2023, 145, 17007-17012.
- 19 D. E. Anderson, A. Tortajada and E. Hevia, Angew. Chem., Int. Ed., 2023, 62, e202218498.
- 20 D. E. Anderson, A. Tortajada and E. Hevia, Angew. Chem., Int. Ed., 2024, 63, e202313556.
- 21 J. Coates, D. Hadi and S. Lincoln, Aust. J. Chem., 1982, 35, 903-909.
- 22 J. Cho, R. Sarangi and W. Nam, Acc. Chem. Res., 2012, 45,
- 23 J. E. Richman and T. J. Atkins, J. Am. Chem. Soc., 1974, 96, 2268-2270.
- 24 T. J. Atkins, J. E. Richman and W. F. Oettle, Org. Synth., 1978, 58, 86.
- 25 J. F. Desreux, E. Merciny and M. F. Loncin, Inorg. Chem., 1981, 20, 987-991.
- 26 G. R. Weisman and D. P. Reed, J. Org. Chem., 1996, 61, 5186-5187.

27 L. E. Lemmerz, D. Mukherjee, T. P. Spaniol, A. Wong, G. Menard, L. Maron and J. Okuda, *Chem. Commun.*, 2019, 55, 3199–3202.

Perspective

- 28 L. J. Morris, P. Ghana, T. Rajeshkumar, A. Carpentier, L. Maron and J. Okuda, *Angew. Chem., Int. Ed.*, 2022, 61, e202114629.
- 29 R. Riedel, A. G. Seel, D. Malko, D. P. Miller, B. T. Sperling, H. Choi, T. F. Headen, E. Zurek, A. Porch, A. Kucernak, N. C. Pyper, P. P. Edwards and A. G. M. Barrett, *J. Am. Chem. Soc.*, 2021, 143, 3934–3943.
- 30 T. X. Gentner and R. E. Mulvey, *Angew. Chem., Int. Ed.*, 2021, **60**, 9247–9262.
- 31 D. E. Anderson, A. Tortajada and E. Hevia, *Angew. Chem., Int. Ed.*, 2023, **62**, e202308766.
- 32 S. Schade and G. Boche, *J. Organomet. Chem.*, 1998, 550, 359–379.
- 33 J. Dyke, W. Levason, M. E. Light, D. Pugh, G. Reid, H. Bhakhoa, P. Ramasami and L. Rhyman, *Dalton Trans.*, 2015, 44, 13853–13866.
- 34 H. Bhakhoa, L. Rhyman, E. P. Lee, D. K. W. Mok, P. Ramasami and J. M. Dyke, *Dalton Trans.*, 2017, 46, 15301–15310.
- 35 H. Osseili, D. Mukherjee, T. P. Spaniol and J. Okuda, *Chem. Eur. J.*, 2017, 23, 14292–14298.
- 36 D. Mukherjee, H. Osseili, T. P. Spaniol and J. Okuda, J. Am. Chem. Soc., 2016, 138, 10790–10793.
- 37 R. Janot, W. S. Tang, D. Clémençon and J. N. Chotard, *J. Mater. Chem.*, 2016, 4, 19045–19052.
- 38 W. S. Tang, J.-N. Chotard, P. Raybaud and R. Janot, *J. Phys. Chem. C*, 2014, **118**, 3409–3419.
- 39 W. S. Tang, J.-N. Chotard, P. Raybaud and R. Janot, *Phys. Chem. Chem. Phys.*, 2012, **14**, 13319–13324.
- 40 J.-N. Chotard, W. S. Tang, P. Raybaud and R. Janot, *Chem. Eur. J.*, 2011, 17, 12302–12309.
- 41 D. Schuhknecht, V. Leich, T. P. Spaniol, I. Douair, L. Maron and J. Okuda, *Chem. Eur. J.*, 2020, **26**, 2821–2825.
- 42 D. Schuhknecht, Doctoral Thesis, RWTH Aachen University, 2020.
- 43 H. Osseili, K.-N. Truong, T. P. Spaniol, D. Mukherjee, U. Englert and J. Okuda, *Chem. Eur. J.*, 2017, 23, 17213–17216.
- 44 D. Schuhknecht, K.-N. Truong, T. P. Spaniol, L. Maron and J. Okuda, *Chem. Commun.*, 2018, **54**, 11280–11283.
- 45 S. Arndt, M. U. Kramer, W. Fegler, Y. Nakajima, I. Del Rosal, R. Poteau, T. P. Spaniol, L. Maron and J. Okuda, *Organometallics*, 2015, 34, 3739–3747.
- 46 W. Fegler, A. Venugopal, T. P. Spaniol, L. Maron and J. Okuda, *Angew. Chem., Int. Ed.*, 2013, 52, 7976–7980.
- 47 L. E. Lemmerz, D. Mukherjee, T. P. Spaniol, A. Wong, G. Ménard, L. Maron and J. Okuda, *Chem. Commun.*, 2019, 55, 3199–3202.
- 48 L. E. Lemmerz, A. Wong, G. Ménard, T. P. Spaniol and J. Okuda, *Polyhedron*, 2020, **178**, 114331.
- 49 D. Schuhknecht, C. Lhotzky, T. P. Spaniol, L. Maron and J. Okuda, *Angew. Chem., Int. Ed.*, 2017, 56, 12367–12371.
- 50 V. Leich, T. P. Spaniol, L. Maron and J. Okuda, *Angew. Chem., Int. Ed.*, 2016, 55, 4794–4797.

- 51 S. Harder, S. Müller and E. Hübner, Organometallics, 2004, 23, 178-183.
- 52 T. Höllerhage, T. P. Spaniol, A. Carpentier, L. Maron and J. Okuda, *Inorg. Chem.*, 2022, **61**, 3309–3316.
- 53 T. Höllerhage, D. Schuhknecht, A. Mistry, T. P. Spaniol, Y. Yang, L. Maron and J. Okuda, *Chem. Eur. J.*, 2021, 27, 3002–3007.
- 54 D. Schuhknecht, T. P. Spaniol, L. Maron and J. Okuda, *Angew. Chem., Int. Ed.*, 2020, **59**, 310–314.
- 55 D. Schuhknecht, T. P. Spaniol, I. Douair, L. Maron and J. Okuda, *Chem. Commun.*, 2019, 55, 14837–14839.
- 56 J. Martin, J. Eyselein, J. Langer, H. Elsen and S. Harder, Chem. Commun., 2020, 56, 9178–9181.
- 57 B. Maitland, M. Wiesinger, J. Langer, G. Ballmann, J. Pahl, H. Elsen, C. Färber and S. Harder, *Angew. Chem.*, *Int. Ed.*, 2017, 56, 11880–11884.
- 58 J. Martin, C. Knüpfer, J. Eyselein, C. Färber, S. Grams, J. Langer, K. Thum, M. Wiesinger and S. Harder, *Angew. Chem.*, *Int. Ed.*, 2020, 59, 9102–9112.
- 59 H. Bauer, M. Alonso, C. Fischer, B. Rösch, H. Elsen and S. Harder, *Angew. Chem.*, *Int. Ed.*, 2018, 57, 15177– 15182.
- 60 E. Le Coz, Z. Zhang, T. Roisnel, L. Cavallo, L. Falivene, J.-F. Carpentier and Y. Sarazin, *Chem. – Eur. J.*, 2020, 26, 3535–3544.
- 61 C. Bellini, V. Dorcet, J.-F. Carpentier, S. Tobisch and Y. Sarazin, *Chem. Eur. J.*, 2016, **22**, 4564–4583.
- 62 C. Bellini, J.-F. Carpentier, S. Tobisch and Y. Sarazin, *Angew. Chem., Int. Ed.*, 2015, **54**, 7679–7683.
- 63 T. Höllerhage, P. Ghana, T. P. Spaniol, A. Carpentier, L. Maron, U. Englert and J. Okuda, *Angew. Chem., Int. Ed.*, 2022, 61, e202115379.
- 64 R. Huo, A. J. Armstrong, G. R. Nelmes, D. J. Lawes, A. J. Edwards, C. L. McMullin and J. Hicks, *Chem. – Eur. J.*, 2024, 30, e202400662.
- 65 D. Schuhknecht, T. P. Spaniol, Y. Yang, L. Maron and J. Okuda, *Inorg. Chem.*, 2020, 59, 9406–9415.
- 66 R. Lalrempuia, C. E. Kefalidis, S. J. Bonyhady, B. Schwarze, L. Maron, A. Stasch and C. Jones, J. Am. Chem. Soc., 2015, 137, 8944–8947.
- 67 M. D. Anker, C. E. Kefalidis, Y. Yang, J. Fang, M. S. Hill, M. F. Mahon and L. Maron, J. Am. Chem. Soc., 2017, 139, 10036–10054.
- 68 M. D. Anker, M. S. Hill, J. P. Lowe and M. F. Mahon, Angew. Chem., Int. Ed., 2015, 54, 10009–10011.
- 69 B. Rösch, T. X. Gentner, H. Elsen, C. A. Fischer, J. Langer, M. Wiesinger and S. Harder, *Angew. Chem., Int. Ed.*, 2019, 58, 5396–5401.
- 70 Z.-W. Qu, H. Zhu and S. Grimme, *Chem. Eur. J.*, 2023, **29**, e202202602.
- 71 X. Shi, G. Qin, Y. Wang, L. Zhao, Z. Liu and J. Cheng, *Angew. Chem., Int. Ed.*, 2019, **58**, 4356–4360.
- 72 Y. Liang, U. K. Das, J. Luo, Y. Diskin-Posner, L. Avram and D. Milstein, *J. Am. Chem. Soc.*, 2022, **144**, 19115–19126.
- 73 Y. Liang, I. Efremenko, Y. Diskin-Posner, L. Avram and D. Milstein, *Angew. Chem., Int. Ed.*, 2024, **63**, e202401702.

74 J. Spielmann, F. Buch and S. Harder, *Angew. Chem., Int. Ed.*, 2008, **47**, 9434–9438.

Dalton Transactions

- 75 A. S. S. Wilson, C. Dinoi, M. S. Hill, M. F. Mahon and L. Maron, *Angew. Chem.*, *Int. Ed.*, 2018, 57, 15500–15504.
- 76 H. Bauer, K. Thum, M. Alonso, C. Fischer and S. Harder, *Angew. Chem.*, *Int. Ed.*, 2019, **58**, 4248–4253.
- 77 H. Bauer, M. Alonso, C. Färber, H. Elsen, J. Pahl, A. Causero, G. Ballmann, F. De Proft and S. Harder, *Nat. Catal.*, 2018, **1**, 40–47.
- 78 A. S. S. Wilson, M. S. Hill and M. F. Mahon, *Organometallics*, 2019, **38**, 351–360.
- 79 L. Garcia, C. Dinoi, M. F. Mahon, L. Maron and M. S. Hill, Chem. Sci., 2019, 10, 8108–8118.
- 80 T. Höllerhage, A. Carpentier, T. P. Spaniol, L. Maron, U. Englert and J. Okuda, *Chem. Commun.*, 2021, 57, 6316–6319.
- 81 C. N. de Bruin-Dickason, T. Sutcliffe, C. Alvarez Lamsfus, G. B. Deacon, L. Maron and C. Jones, *Chem. Commun.*, 2018, 54, 786–789.
- 82 D. Mukherjee, T. Höllerhage, V. Leich, T. P. Spaniol, U. Englert, L. Maron and J. Okuda, *J. Am. Chem. Soc.*, 2018, 140, 3403–3411.
- 83 X. Sun and A. Hinz, *Inorg. Chem.*, 2023, **62**, 10249–10255.
- 84 M. C. Lipke and T. D. Tilley, *Angew. Chem., Int. Ed.*, 2012, 51, 11115–11121.
- 85 M. S. Hill, M. F. Mahon, A. S. S. Wilson, C. Dinoi, L. Maron and E. Richards, *Chem. Commun.*, 2019, 55, 5732–5735.
- 86 P. M. Chapple and Y. Sarazin, Eur. J. Inorg. Chem., 2020, 3321–3346.
- 87 T. Höllerhage, T. P. Spaniol, U. Englert and J. Okuda, Z. Anorg. Allg. Chem., 2023, 649, e202200315.
- 88 M. Wiesinger, B. Maitland, C. Färber, G. Ballmann, C. Fischer, H. Elsen and S. Harder, *Angew. Chem., Int. Ed.*, 2017, **56**, 16654–16659.
- 89 X. Shi, C. Hou, C. Zhou, Y. Song and J. Cheng, *Angew. Chem., Int. Ed.*, 2017, **56**, 16650–16653.
- T. Höllerhage, T. P. Spaniol, U. Englert and J. Okuda, Inorg. Chim. Acta, 2022, 543, 121198.
- 91 R. D. Hancock, P. W. Wade, M. P. Ngwenya, A. S. De Sousa and K. V. Damu, *Inorg. Chem.*, 1990, **29**, 1968–1974.
- 92 M. T. S. Amorim, S. Chaves, R. Delgado and J. J. R. F. da Silva, *J. Chem. Soc., Dalton Trans.*, 1991, 3065–3072.
- 93 R. D. Shannon, *Acta Crystallogr., Sect. A: Found. Adv.*, 1976, 32, 751–767.
- 94 D. Mukherjee, A. K. Wiegand, T. P. Spaniol and J. Okuda, *Dalton Trans.*, 2017, 46, 6183–6186.
- 95 H. H. Cui, W. Lv, W. Tong, X. T. Chen and Z. L. Xue, *Eur. J. Inorg. Chem.*, 2019, 4653–4659.
- 96 H. H. Cui, J. Wang, X. T. Chen and Z. L. Xue, *Chem. Commun.*, 2017, 53, 9304–9307.
- 97 M. X. Xu, Z. Liu, B. W. Dong, H. H. Cui, Y. X. Wang, J. Su, Z. X. Wang, Y. Song, X. T. Chen, S. D. Jiang and S. Gao, *Inorg. Chem.*, 2019, 58, 2330–2335.
- 98 F. Ritter, L. J. Morris, K. N. McCabe, T. P. Spaniol, L. Maron and J. Okuda, *Inorg. Chem.*, 2021, **60**, 15583– 15592.

- 99 F. Ritter, Doctoral Thesis, RWTH Aachen University, 2021.
- D. Mukherjee, S. Shirase, T. P. Spaniol, K. Mashima and J. Okuda, *Chem. Commun.*, 2016, 52, 13155–13158.
- 101 F. Ritter, T. P. Spaniol, I. Douair, L. Maron and J. Okuda, Angew. Chem., Int. Ed., 2020, 59, 23335–23342.
- 102 R. Chambenahalli, R. M. Bhargav, K. N. McCabe, A. P. Andrews, F. Ritter, J. Okuda, L. Maron and A. Venugopal, *Chem. – Eur. J.*, 2021, 27, 7391–7401.
- 103 P. Mahawar, T. Rajeshkumar, T. P. Spaniol, L. Maron and J. Okuda, *Chem. Commun.*, 2024, **60**, 11359–11362.
- 104 S. Schulz, D. Schuchmann, I. Krossing, D. Himmel, D. Bläser and R. Boese, *Angew. Chem., Int. Ed.*, 2009, **48**, 5748–5751.
- 105 H. Banh, C. Gemel, R. W. Seidel and R. A. Fischer, *Chem. Commun.*, 2015, 51, 2170–2172.
- 106 J. L. Atwood, K. D. Robinson, C. Jones and C. L. Raston, J. Chem. Soc., Chem. Commun., 1991, 1697–1699.
- 107 P. Dabringhaus and I. Krossing, Chem. Sci., 2022, 13, 12078–12086.
- 108 R. J. Wehmschulte, R. Peverati and D. R. Powell, *Inorg. Chem.*, 2019, 58, 12441–12445.
- 109 M. Schorpp, R. Tamim and I. Krossing, *Dalton Trans.*, 2021, **50**, 15103–15110.
- 110 J. L. Bourque, R. A. Nanni, M. C. Biesinger and K. M. Baines, *Inorg. Chem.*, 2021, **60**, 14713–14720.
- 111 M. Everett, A. Jolleys, W. Levason, M. E. Light, D. Pugh and G. Reid, *Dalton Trans.*, 2015, 44, 20898–20905.
- 112 J. M. Slattery, A. Higelin, T. Bayer and I. Krossing, *Angew. Chem., Int. Ed.*, 2010, **49**, 3228–3231.
- 113 J. T. Boronski, M. P. Stevens, B. van Ijzendoorn, A. C. Whitwood and J. M. Slattery, *Angew. Chem., Int. Ed.*, 2021, **60**, 1567–1572.
- 114 C. G. Andrews and C. L. B. Macdonald, *Angew. Chem., Int. Ed.*, 2005, **44**, 7453–7456.
- 115 A. Higelin, C. Haber, S. Meier and I. Krossing, *Dalton Trans.*, 2012, **41**, 12011–12015.
- 116 A. Barthelemy, K. Glootz, H. Scherer, A. Hanske and I. Krossing, *Chem. Sci.*, 2022, **13**, 439–453.
- 117 Z. L. Li, G. Thiery, M. R. Lichtenthaler, R. Guillot, I. Krossing, V. Gandon and C. Bour, *Adv. Synth. Catal.*, 2018, **360**, 544–549.
- 118 Z. L. Li, S. W. Yang, G. Thiery, V. Gandon and C. Bour, J. Org. Chem., 2020, 85, 12947–12959.
- 119 P. Dabringhaus, A. Barthelemy and I. Krossing, *Z. Anorg. Allg. Chem.*, 2021, **647**, 1660–1673.
- 120 K. Glootz, D. Kratzert, D. Himmel, A. Kastro, Z. Yassine, T. Findeisen and I. Krossing, *Angew. Chem., Int. Ed.*, 2018, 57, 14203–14206.
- 121 M. R. Lichtenthaler, F. Stahl, D. Kratzert, L. Heidinger, E. Schleicher, J. Hamann, D. Himmel, S. Weber and I. Krossing, *Nat. Commun.*, 2015, 6, 8288.
- 122 C. Dohmeier, D. Loos and H. Schnockel, Angew. Chem., Int. Ed. Engl., 1996, 35, 129–149.
- 123 J. C. Beamish, A. Boardman and I. J. Worrall, *Polyhedron*, 1991, **10**, 95–99.
- 124 L. J. Morris, P. Mahawar and J. Okuda, *J. Org. Chem.*, 2022, **80**, 5090–5096.

125 M. Auer, F. Diab, K. Eichele, H. Schubert and L. Wesemann, *Dalton Trans.*, 2022, **51**, 5950–5961.

Perspective

- 126 J. J. Maudrich, F. Diab, S. Weiss, M. Widemann, T. Dema, H. Schubert, K. M. Krebs, K. Eichele and L. Wesemann, *Inorg. Chem.*, 2019, **58**, 15758–15768.
- 127 K. R. Cairns, R. P. King, R. D. Bannister, W. Levason and G. Reid, *Dalton Trans.*, 2023, 52, 2293–2308.
- 128 A. Higelin, U. Sachs, S. Keller and I. Krossing, *Chem. Eur. J.*, 2012, **18**, 10029–10034.
- 129 A. Barthélemy, H. Scherer, H. Weller and I. Krossing, *Chem. Commun.*, 2023, **59**, 1353–1356.
- 130 A. Barthélemy, H. Scherer, M. Daub, A. Bugnet and I. Krossing, *Angew. Chem.*, *Int. Ed.*, 2023, **62**, e202311648.
- 131 A. Barthélemy, H. Scherer and I. Krossing, *Chem. Eur. J.*, 2022, **28**, e202201369.

- 132 P. Dabringhaus, H. Scherer and I. Krossing, *Nat. Synth.*, 2024, 3, 732–743.
- 133 P. A. Rupar, V. N. Staroverov and K. M. Baines, *Science*, 2008, 322, 1360–1363.
- 134 F. Cheng, A. L. Hector, W. Levason, G. Reid, M. Webster and W. Zhang, *Angew. Chem.*, *Int. Ed.*, 2009, 48, 5152– 5154.
- 135 P. A. Rupar, R. Bandyopadhyay, B. F. T. Cooper, M. R. Stinchcombe, P. J. Ragogna, C. L. B. Macdonald and K. M. Baines, *Angew. Chem., Int. Ed.*, 2009, 48, 5155–5158.
- 136 R. P. King, J. M. Herniman, W. Levason and G. Reid, *Inorg. Chem.*, 2023, **62**, 853–862.
- 137 D. Mukherjee, D. Schuhknecht and J. Okuda, *Angew. Chem., Int. Ed.*, 2018, 57, 9590–9602.
- 138 M. M. D. Roy, A. A. Omana, A. A. S. Wilson, M. S. Hill, S. Aldridge and E. Rivard, *Chem. Rev.*, 2021, **121**, 12784–12965.